Neotropical Ichthyology

Original article

https://doi.org/10.1590/1982-0224-2023-0095

urn:lsid:zoobank.org:pub:E4F38021-20D6-452D-8E7D-83234E442A95

Integrative taxonomy of the black-barred disk pacus (Characiformes: Serrasalmidae), including the redescription of *Myloplus schomburgkii* and the description of two new species

Correspondence:
Victória D. Pereira
vdps.097@gmail.com

Valéria N. Machado[1], Victória D. Pereira[2], Rafaela P. Ota[3], Rupert A. Collins[4], Marcelo Ândrade[5], James R. Garcia-Ayala[2], Michel Jégu[6,7], Izeni P. Farias[1] and Tomas Hrbek[1,7]

Presently, *Myloplus schomburgkii* is the most easily recognized species among the serrasalmids by having a vertical black bar in the middle of the body. However, through a broad taxonomic review, including DNA barcoding and morphological analyses, we were able to identify and describe two new species that also share a dark vertical bar on the flank. In addition, we redescribe *M. schomburgkii*, designating a neotype and restricting the type-locality to rio Negro in Barcelos, Amazonas State, Brazil. The three lineages of black-barred pacus present high molecular divergences (7.9–11%) and can be distinguished by differences in the shape of the vertical bar, shape of females' anal fin, number of total vertebrae, number of total branched dorsal-fin rays, among other characters. Although the existence of these two new species has been hidden due to many morphological similarities, mainly the presence of the black bar, the three lineages do not compose a monophyletic group, with one of the new species being recovered as sister to *Ossubtus xinguense*. This result reinforces the necessity of the redefinition of the Myleini genera.

Keywords: Amazon basin, COI, DNA barcoding, Myleini, Neotype.

Submitted August 15, 2023
Accepted February 19, 2024
by Bruno Melo
Epub June 10, 2024

1 Laboratório de Evolução e Genética Animal (LEGAL), Departamento de Genética, Universidade Federal do Amazonas (UFAM), Av. Gal. Octávio Jordão Ramos, 6200, 69080-900 Manaus, AM, Brazil. (VNM) valeria.pesca@gmail.com, (IPF) izeni@evoamazon.net, (TH) tomas@evoamazon.net.

2 Laboratório de Biologia e Genética de Peixes, Setor Morfologia, Universidade Paulista "Júlio de Mesquita Filho", Instituto de Biociências da Unesp de Botucatu, Rua Professor Doutor Antônio Celso Wagner Zanin, 250, 18618-689 Botucatu, SP, Brazil. (VDP) vdps.097@gmail.com (corresponding author), (JRGA) james.ayala@unesp.br.

3 Museu da Biodiversidade, Laboratório de Biogeografia e Sistemática de Peixes (LABISPE), Universidade Federal da Grande Dourados (UFGD), Rodovia Dourados-Itahum, km 12, 79804-970 Dourados, MS, Brazil. (RPO) rafaelaota@ufgd.edu.br.

4 Department of Life Sciences, Natural History Museum, London, United Kingdom. (RAC) rupert.collins@nhm.ac.uk.

5 Centro de Ciências Humanas, Naturais, Saúde e Tecnologia, Universidade Federal do Maranhão (UFMA), Rodovia Pinheiro-Pacas, km 10, 65200-000 Pinheiro, MA, Brazil. (MA) mc.andrade@ufma.br.

6 Institut de Recherche pour le Développement, Biologie des Organismes et Ecosystèmes Aquatiques, Laboratoire d´Icthyologie, Muséum National d'Histoire Naturelle, C.P. 26, 43 rue Cuvier, 75231 Paris, France. (MJ) michel.jegu@gmail.com.

7 Biology Department, Trinity University, 78212 San Antonio, TX, United States of America.

Online version ISSN 1982-0224
Print version ISSN 1679-6225

Neotrop. Ichthyol.
vol. 22, no. 2, Maringá 2024

Atualmente, *Myloplus schomburgkii* representa a espécie mais facilmente reconhecida entre os serrasalmídeos, por apresentar uma barra preta vertical no meio do corpo. No entanto, através de uma ampla revisão taxonômica, incluindo DNA barcoding e análises morfológicas, conseguimos identificar e descrever duas novas espécies que também compartilham a barra vertical escura no flanco. Além disso, redescrevemos *M. schomburgkii*, designando um neótipo e restringindo a localidade-tipo ao rio Negro, Barcelos, Estado do Amazonas, Brasil. As três linhagens de pacus de barra preta apresentam altas divergências moleculares (7,9–11%) e podem ser morfologicamente distinguidas por diferenças na forma da barra vertical, forma da nadadeira anal nas fêmeas, número de vértebras totais, número de raios ramificados na nadadeira dorsal, entre outros caracteres. Embora a existência dessas duas novas espécies tenha sido ocultada devido a grandes semelhanças morfológicas, principalmente pela presença da barra vertical preta, as três linhagens não compõem um grupo monofilético, com uma das novas espécies sendo recuperada como irmã de *Ossubtus xinguense*. Este resultado reforça a necessidade da redefinição dos gêneros de Myleini.

Palavras-chave: Bacia Amazônica, COI, DNA barcode, Myleini, Neótipo.

INTRODUCTION

The species diversity and phylogenetic relationships within the piranha and pacu family Serrasalmidae is becoming better understood as geographic sampling has increased (Machado *et al*., 2018), more powerful phylogenomic analyses are performed (Kolmann *et al*., 2020; Mateussi *et al*., 2020), and taxonomic efforts are expedited (*e.g*., Andrade *et al*., 2019; Ota *et al*., 2020). One particular group has remained difficult, however. Since the proposition of the "*Myleus* clade" by Ortí *et al*. (1996) (=Myleinae *sensu* Kolmann *et al*., 2020; =Myleini *sensu* Mateussi *et al*., 2020), to allocate *Myloplus* Gill, 1896, *Myleus* Müller & Troschel, 1844, *Mylesinus* Valenciennes, 1850, and *Tometes* Valenciennes, 1850, several studies have tried to clarify the relationships among these pacus (Thompson *et al*., 2014; Andrade *et al*., 2016a; Kolmann *et al*., 2020; Mateussi *et al*., 2020), but their limits remain unclear.

Myloplus, the third most species-rich genus within Serrasalmidae, comprises the colloquially known pacus, and is currently represented by 12 valid species widely distributed in South America (Andrade *et al*., 2016b; Kolmann *et al*., 2020; Fricke *et al*., 2023). The genus has been traditionally diagnosed by tooth arrangement, mainly by the presence of a gap between labial and lingual premaxillary rows of teeth; and the lack of contact between contralateral labial tooth rows at the symphysis (Jégu *et al*., 2004; Andrade *et al*., 2016b). However, recent molecular phylogenetic studies recovered *Myloplus* as polyphyletic, suggesting that the morphological similarities among its species probably arose by adaptive convergence related to feeding habits (Kolmann *et al*., 2020; Mateussi *et al*., 2020).

In their recent molecular phylogeny of Serrasalmidae using exon-capture phylogenomic methods, Kolmann *et al*. (2020) raised the three major groups within the

family — previously proposed by Ortí *et al*. (2008) as the "pacu clade", "*Myleus* clade", and "piranha clade" — to the subfamilies Colossomatinae, Myleinae, and Serrasalminae. *Myloplus* was recovered within Myleinae, but polyphyletic. To solve the polyphyly of *Myloplus*, the authors raised to full generic rank the former subgenus *Prosomyleus* Géry, 1972, which includes only *Prosomyleus rhomboidalis* (Cuvier, 1818), sister to the remaining Myleinae, except *Acnodon* Eigenmann, 1903. They also resurrected *Paramyloplus* Norman, 1929, including *Paramyloplus ternetzi* Norman, 1929 and *Paramyloplus taphorni* (Andrade, López-Fernández & Liverpool, 2019), which is sister to a clade formed by *Myloplus sensu stricto* [*i.e*., the type-species *M. asterias* (Müller & Troschel, 1844) and the closely-related *M. lobatus* (Valenciennes, 1850), *M. rubripinnis* (Müller & Troschel, 1844), *M. torquatus* (Kner, 1858)] and *Utiaritichthys* Miranda Ribeiro, 1937. This clade including *Paramyloplus*, *Utiaritichthys*, and *Myloplus sensu stricto* is sister to a larger clade that encompasses species of *Ossubtus* Jégu, 1992, *Tometes*, *Mylesinus*, and *Myleus*, among which are nested '*Myloplus*' *schomburgkii* (Jardine, 1841), '*M.*'*arnoldi* Ahl, 1936, '*M.*' *lucienae* Andrade, Ota, Bastos & Jégu, 2016 and '*M.*' *planquettei* (Jégu, Keith & Le Bail, 2003). More recently, Mateussi *et al*. (2020) in a molecular phylogeny using ultraconserved elements (UCEs), propose the division of Serrasalmidae into just two subfamilies: Colossomatinae and Serrasalminae, the latter being subdivided into two tribes: Myleini and Serrasalmini. In this phylogeny, the "*Myleus* group" falls within the Myleini tribe which also includes *Acnodon.* All genera remain polyphyletic, with the exception of *Ossubtus*, which is monotypic.

Despite these new arrangements, the evolutionary relations of *Myloplus* remain unsolved. The genus lacks a proper morphological diagnosis, and several species still await a new generic designation. One of them is '*Myloplus*' *schomburgkii*, recovered as sister to the monotypic *Ossubtus xinguense* Jégu, 1992.

The sisterhood between '*Myloplus*' *schomburgkii* and the monotypic *Ossubtus* was recovered by Machado *et al*. (2018), Kolmann *et al*. (2020) and Mateussi *et al*. (2020). However, the inclusion of '*M.*' *schomburgkii* in *Ossubtus* was not considered for two reasons. First, the species lacks the several autapomorphic conditions defining the genus (*e.g*., subinferior to inferior mouth; absence of spines on prepelvic serrae; four infraorbitals; narrow incisiform teeth, flattened anteroposteriorly, and weakly attached to jaws; premaxillary teeth rows in contact with each other, the first two labial premaxillary teeth with reduced crown; four teeth on dentary) (Jégu, 1992). Second, given the polyphyletic nature of '*M.*' *schomburgkii*, it is necessary first to determine whether the lineage sampled in these studies corresponds to typical '*M.*' *schomburgkii* or to another, undescribed species.

'*Myloplus*' *schomburgkii* has always been considered a species of easy morphological identification, with a distinct vertical black bar in the middle of the body, inspiring the vernacular names "black-barred disk pacu", "black-barred myleus", black-barred silver dollar", and "black-banded pacu". Since its description by Jardine (1841) this species has never been revisited, mainly due to the apparent easy recognition. However, more recent studies of the Serrasalmidae, especially molecular, have shown the presence of genetically distinct lineages within this taxon (Machado *et al*., 2018; Kolmann *et al*., 2020). Machado *et al*. (2018) recovered four and Kolmann *et al*. (2020) three lineages within *Myloplus schomburgkii*.

Therefore, through an integrative approach, using molecular and morphological characters, the objectives of the present study are: (i) to delimit the lineages within the "*Myloplus schomburgkii*" complex based on DNA barcode, (ii) to redescribe *M. schomburgkii* designating a neotype, and (iii) describe two new species previously misidentified as *M. schomburgkii*.

MATERIAL AND METHODS

Morphological analysis. Counts and measurements were taken as in the former papers of descriptions of *Myloplus* species (*e.g.*, Jégu *et al.*, 2003, 2004; Andrade *et al.*, 2016a,b; Ota *et al.*, 2020), with addition of the adipose-fin length, taken from the last scales row covering the adipose-fin base origin to its distal tip. Measurements, which are presented as percentages of standard length (SL) and head length (HL), were taken with a digital caliper to the nearest 0.1 mm between landmarks, as described in Fig. 1, and Tab. 1. Counts were taken under a stereomicroscope. The ventral keel count comprises prepelvic spines (all those preceding the pelvic-fin insertion), postpelvic spines (those posterior to pelvic-fin insertion), and the paired spines around anus. Osteological terminology follows Mattox *et al.* (2014). Counts of vertebrae, supraneurals, pterygiophores, and ventral keel spines, as shape and position of these osteological structures were obtained from radiographed (x-ray) specimens taken in Faxitron®radiography system LX-60 (www.faxitron.com) 40 kV. Vertebrae counts include those of the Weberian apparatus as four elements, and the fused PU1+U1 as a single centrum.

In the description section, counts of holotypes and neotype are indicated by an asterisk, and numbers in parentheses indicate the frequency of the counts. The choice of type-material was based on the size and preservation of the specimens (*i.e.*, specimens smaller than 40 mm SL or those with any type of damage, such as missing fins or open specimens, were not selected). In the analyzed material lists, the number of specimens is followed by x-rayed, tissue voucher number (CTGA - Coleção de Tecidos de Genética Animal), and by GenBank accession number in parentheses. Institutional abbreviations are: ANSP, Academy of Natural Sciences of Philadelphia, Philadelphia; BMNH, Natural History Museum, London; CIIAP, Colección Ictiológica del Instituto de Investigaciones de la Amazonía Peruana, Iquitos; INPA, Instituto Nacional de Pesquisas da Amazônia, Manaus; LBP, Laboratório de Biologia e Genética de Peixes, Instituto de Biociências, Unesp, Botucatu; MNRJ, Museu Nacional, Universidade Federal do Rio de Janeiro, Rio de Janeiro; MUBIO, Museu da Biodiversidade, Universidade Federal da Grande Dourados, Dourados; MZUSP, Museu de Zoologia da Universidade de São Paulo, São Paulo; NMW, Naturhistorisches Museum Zoologische Abteilung, Fische, Vienna; NUP, Núcleo de Pesquisas em Limnologia, Ictiologia e Aquicultura, Maringá; and ZUFMS, Coleção Zoológica de Referência da Universidade Federal de Mato Grosso do Sul, Campo Grande.

Molecular analysis. For the molecular analyses we obtained available COI (mitochondrial cytochrome *c* oxidase subunit I) DNA barcode sequences from the GenBank (https://www.ncbi.nlm.nih.gov/nucleotide) and BOLD (https://www.boldsystems.org/) databases, as published in previous studies (Machado *et al.*, 2018; Ota

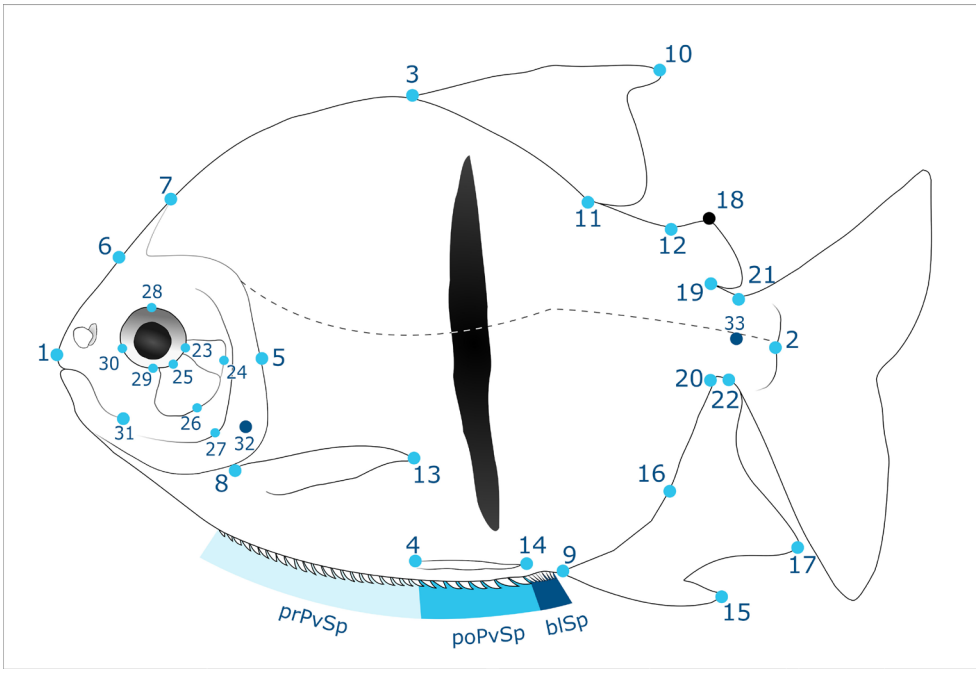

FIGURE 1 | Schematic drawing of *Myloplus schomburgkii* with the landmarks used in the measurements. 1, anteriormost point of the snout. 2, distal margin of the hypurals. 3, dorsal-fin insertion. 4, pelvic-fin insertion. 5, posteriormost point of the opercle, not including opercular membrane. 6, supraoccipital's base. 7, supraoccipital's distal tip. 8, pectoral-fin insertion. 9, anal-fin insertion. 10, distal tip of the longest dorsal-fin unbranched ray. 11, base of the last dorsal-fin ray. 12, anterior end of the adipose-fin base. 13, pectoral-fin distal tip. 14, pelvic-fin distal tip. 15, distal tip of the longest anal-fin unbranched ray. 16, base of the longest ray of the second anal-fin lobe. 17, distal tip of the longest branched ray of the second anal-fin lobe. 18, distal end of the anterodorsal margin of the adipose fin. 19, posterior end of the adipose-fin base. 20, posterior end of the anal-fin base. 21, point of the dorsal profile of the caudal peduncle in which it is closest to ventral profile. 22, point of the ventral profile of the caudal peduncle in which it is closest to dorsal profile. 23, posteriormost point of the eye. 24, middle of posterior margin of the fourth infraorbital. 25, middle of anterodorsal margin of third infraorbital. 26, middle of posteroventral margin of third infraorbital. 27, internal angle of pre-opercle. 28, dorsalmost point of the eye. 29, ventralmost point of the eye. 30, anteriormost point of the eye. 31, distal end of the premaxilla. 32, point in which the head is wider. 33, point in which the caudal peduncle is wider. The ventral keel count comprises prepelvic spines (prPvSp), postpelvic spines (poPvSp), and the paired spines around anus (bISp).

et al., 2020; Papa *et al*., 2021; García-Dávila *et al*., 2022). In addition, we generated new COI sequence data for additional putative "*Myloplus schomburgkii*" individuals from collections. For phylogenetic context we included representatives of all nine genera (*Myloplus*, *Myleus*, *Mylesinus*, *Ossubtus*, *Tometes*, *Utiaritichthys*, *Paramyloplus*, *Prosomyleus*, and *Acnodon*) of the Myleini *sensu* Mateussi *et al*. (2020), Myleinae *sensu* Kolmann *et al*. (2020) and the "teal" lineage of Thompson *et al*. (2014). The analysis included 31 species, which are all listed in Tab. 2.

TABLE 1 | Description of the measurements. The numbers in parentheses correspond to the landmarks. Numbers followed by (') corresponds to landmarks on the right side of the fish.

Measurements	Description of the measurements with the landmarks
Standard length	From the anteriormost point of the snout (1) to the distal margin of the hypurals (2)
Body depth	From dorsal-fin insertion (3) to the pelvic-fin insertion (4)
Head length	From the anteriormost point of the snout (1) to the posteriormost point of the opercle, not including the opercular membrane (5)
Supraoccipital process	From the Supraocciptal's base (6) to the Supraocciptal's distal tip (7)
Predorsal length	From the anteriormost point of the snout (1) to the dorsal-fin insertion (3)
Postdorsal length	From the dorsal-fin insertion (3) to the distal margin of the hypurals (2)
Prepectoral length	From the anteriormost point of the snout (1) to the pectoral-fin insertion (8)
Prepelvic length	From the anteriormost point of the snout (1) to the pelvic-fin insertion (4)
Preanal length	From the anteriormost point of the snout (1) to the anal-fin insertion (9)
Dorsal-fin length	From the dorsal-fin insertion (3) to the distal tip of the longest dorsal-fin unbranched ray (10)
Interdorsal length	From the dorsal-fin origin (11) to the anterior end of the adipose-fin base (12)
Pectoral-fin length	From the pectoral-fin insertion (8) to the pectoral-fin distal tip (13)
Pelvic-fin length	From the pelvic-fin insertion (4) to the pelvic-fin distal tip (14)
First anal-fin lobe length	From the anal-fin insertion (9) to the distal tip of the longest anal-fin unbranched ray (15)
Second anal-fin lobe length	From the base of the longest branched ray of the second anal-fin lobe (16) to its tip (17)
Adipose-fin length	From the anterior end of the adipose-fin base (12) to the distal end of the anterodorsal margin of the adipose fin (18)
Dorsal-fin base length	From the dorsal-fin insertion (3) to the dorsal-fin origin (11)
Adipose-fin base length	From the anterior end of the adipose-fin base (12) to the posterior end of the adipose-fin base (19)
Anal-fin base length	From the anal-fin insertion (9) to the posterior end of the anal-fin base (20)
Caudal-peduncle depth	The shortest distance between the dorsal and ventral profiles of the caudal peduncle (21 to 22')
Width of peduncle	Point in which the caudal peduncle is wider (33 to 33')
Supraoccipital to dorsal-fin	From the supraocciptal's base (6) to the dorsal-fin insertion (3)
Snout to Supraoccipital	From the anteriormost point of the snout (1) to the supraocciptal's distal tip (7)
Snout to base of supraocciptal	From the anteriormost point of the snout (1) to the supraocciptal's base (6)
Pelvic-anal distance	From the pelvic-fin insertion (4) to the anal-fin insertion (9)
Pectoral-pelvic distance	From the pectoral-fin insertion (8) to the pelvic-fin insertion (4)
Dorsal-fin origin to anal-fin origin	From the dorsal-fin insertion (3) to the anal-fin insertion (9)
Dorsal-fin end to anal-fin origin	From the dorsal-fin origin (11) to the anal-fin insertion (9)
Dorsal-fin end to anal-fin end	From the dorsal-fin origin (11) to the posterior end of the anal-fin base (20)
Head width	Point in which the head is wider (32 to 32')
Postorbital distance	From the posteriormost margin of the eye (23) to the posteriormost point of the opercle, not including the opercular membrane (5)
Fourth infraorbital width	From the middle point of the anteromargin of the fourth infraorbital (23) to the middle point of its posterior margin (24)
Third infraorbital width	From the middle point of the anterordorsal margin of the third infraorbital (25) to the middle point of its posteroventral margin (26)
Cheek gap width	From the middle point of the third infraorbital posteroventral margin (26) to the internal angle of the preopercle (27)
Interorbital width	Between the dorsalmost point of the orbits (28 to 28')
Eye vertical diameter	From the dorsalmost point of the orbit (28) to its ventralmost point (29)
Snout length	From the anteriormost point of the snout (1) to the anteriormost point of the orbit (30)
Mouth length	From the anteriormost point of the snout (1) to the distal end of the maxilla (31)
Mouth width	Between the distal tip of the maxillae (31 to 31')

Laboratory protocols for DNA extraction, PCR, and Sanger sequencing followed Machado *et al*. (2018). Tissue samples were stored in 95% ethanol and deposited in the CTGA collection of UFAM, while corresponding voucher specimens were fixed in 10% formalin and deposited in the fish collection of INPA. The sequence chromatograms were assembled and trimmed in Geneious 7.0.6 (Kearse *et al*., 2012). Resulting sequences

were aligned using MAFFT v. 7.490 (Katoh, Standley, 2013), and the alignment quality controlled by amino acid translation (Geneious), and neighbor-joining (p-distances, pairwise deletion) trees in R v. 4.2.1 using the Ape v. 5.6.2 (Paradis, Schliep, 2019) package.

To estimate species alpha diversity from the COI data, we used the mPTP species discovery method (Kapli *et al.*, 2017). First, the sequence data was dereplicated, *i.e.*, collapsed into unique haplotypes, and where sequences were otherwise identical but differed in length due to end trimming, the longer sequence was retained. The input phylogenetic tree for mPTP was constructed using MrBayes v. 3.2.7a (Ronquist *et al.*, 2012). Appropriate substitution model (GTR+G) was selected by AIC in jModelTest v. 2.1.10 (Darriba *et al.*, 2012). Unconstrained compound-dirichlet branch-length priors were used following Zhang *et al.* (2012). Four independent unheated chains were run from random starting topologies for 10 million generations. Chains were sampled every 3,600 generations and a burnin of 10% was applied, resulting in 10,000 post-burnin posterior trees over the four chains. Chain convergence was assessed with Tracer v. 1.7.2 (https://github.com/beast-dev/tracer/). The post-burnin trees were summarized into a maximum clade credibility (MCC) topology (common ancestor node heights)

TABLE 2 | Summary by species of samples used in the molecular analysis.

Species	Number samples	Number drainages	Number localities	Number haplotypes
Acnodon normani	2	1	1	2
Acnodon oligacanthus	15	1	6	5
Acnodon senai	2	1	1	1
Mylesinus paraschomburgkii	15	3	3	4
Mylesinus paucisquamatus	5	2	2	3
Myleus micans	7	1	3	5
Myleus planquettei	7	2	6	4
Myleus setiger	29	8	14	13
Myloplus arnoldi	24	5	11	8
Myloplus asterias	21	7	9	15
Myloplus levis	2	1	1	1
Myloplus lobatus	31	5	8	7
Myloplus lucienae	6	1	4	1
Myloplus nigrolineatus	68	11	18	20
Myloplus rubripinnis	49	6	13	16
Myloplus schomburgkii	89	13	32	36
Myloplus sp.	35	6	11	16
Myloplus tiete	1	1	1	1
Myloplus zorroi	14	1	2	4
Ossubtus xinguense	6	1	3	4
Paramyloplus ternetzi	33	1	11	4
Prosomyleus rhomboidalis	33	4	13	7
Tometes ancylorhynchus	8	1	2	4
Tometes camunani	6	2	4	4
Tometes kranponhah	13	2	3	4
Tometes lebaili	13	1	8	6
Tometes makue	1	1	1	1
Tometes siderocarajensis	8	3	5	4
Tometes sp.	15	1	3	6
Tometes trilobatus	1	1	1	1
Utiaritichthys longidorsalis	5	1	1	2

using Tree Annotator v. 1.10.4 (https://github.com/beast-dev/beast-mcmc). Trees were midpoint rooted on the longest internal edge in Phangorn v. 2.10.0 (Schliep, 2011). The MCC topology was run in mPTP (single threshold) to generate a point estimate of species alpha diversity. To account for branch length and topological uncertainty in the species estimations, we randomly subsampled 1,000 of the post-burnin posterior tree sample and conducted the same mPTP analysis over these trees. The frequency of the individual delimitations in the MCC tree that were shared in the posterior tree subsample represents the Bayesian posterior probability (BPP) support for those delimitations. The Spider v. 1.5.0 package (Brown *et al*., 2012) was used to summarize the p-distances within and between the putative species.

All data and code to repeat the analyses is available at the following: https://doi.org/10.5281/zenodo.10032056. All newly generated sequence data are deposited in the GenBank nucleotide database (https://www.ncbi.nlm.nih.gov/nucleotide) under accession numbers OR366865 to OR366904.

RESULTS

Myloplus aylan Pereira, Ota, Machado, Collins, Ândrade, Garcia-Ayala, Jégu, Farias & Hrbek, new species

urn:lsid:zoobank.org:act:2EF3345A-B36F-4BC7-9507-FFECBEB043FC

(Figs. 2–5; Tab. 3)

Prosomyleus (*Myleus*) *schomburgkii* Géry, 1977:266 [listed, brief description of the subgenus; photo in page 269, above; locality: Alto Solimões (Brazil)].

Myleus schomburgkii. —Machado-Allison, Fink, 1995:62–63 [cover figure; brief description; illustration, fig. 26:63; locality: Orinoco and Casiquiare rivers (Venezuela)] —Vari *et al*., 2009:72 [listed; photo F; locality: Orinoco (Venezuela)].

Myloplus schomburgkii. —Murrieta-Morey *et al*., 2019:511–19 [description of a new species of parasite, locality: Rio Nanay basin (Peru)]. —Murrieta-Morey *et al*., 2021:110 [mortality and water quality; figs. 1C, D; locality: Rio Nanay basin]. —Kolmann *et al*., 2020:2 [exon-based phylogeny; fig. 1]. —Mateussi *et al*., 2020:3 [Listed].

Holotype. INPA 60150, male, 213.01 mm SL, A3742 (GenBank accession OR366877), Brazil, Roraima, Caracaraí municipality, rio Baraúna, lago do Bento, 01°15'34.4"N 60°54'32.4"W, 17 Jan 2021, M. S. Rocha.

Paratypes. Brazil: Amazonas: Apuí: INPA 60151, 1, 91.32 mm SL, rio Guariba tributary of Aripuanã basin, at Reserva Extrativista do Guariba, 08°42'42"S 60°25'53"W, 7 Aug 2008, W. S. Pedroza, W. Ohara, F. R. Ribeiro & T. F. Teixeira. INPA 60153, 1, 81.97 mm SL, rio Guariba at Reserva Extrativista do Guariba, 08°42'42"S 60°25'53"W, 14 Nov 2008, W. S. Pedroza, W. Ohara, F. R. Ribeiro & T. F. Teixeira. **Carauari:** INPA 60673, 1, 185.0 mm SL, (CTGA 22529), Igarapé Pucá tributary of rio Juruá, 02°50'40"S 66°57'51"W, 1 Jul 2022, T. Hrbek. **Careiro:** INPA 60702, 1, 131.2 mm

FIGURE 2 | *Myloplus aylan*, INPA 60150, holotype, male, 213.01 mm SL, Brazil, Roraima, Caracaraí municipality, rio Baraúna, lago do Bento.

SL, (CTGA 22278), rio Juma, interfluve of Madeira-Purus, 03°42'19"S 59°48'46"W, 26 Sep 2021, V. N. Machado. **Jutaí:** INPA 60672, 1, 178.1 mm SL, (CTGA 22524), rio Jutaí, 04°46'12"S 66°37'06"W, 1 Sep 2022, V. N. Machado. INPA 60709, 1, 155.3 mm SL, (CTGA 23316), rio Jutaí, 02°54'13"S 67°02'35"W, 10 Fev 2023, V. N. Machado. BMNH 2024.2.12.1-2, 2, 171.0–187.1 mm SL, (CTGA 22523, 22525) same collection data as INPA 60672. **Presidente Figueiredo:** INPA 22192, 2, 275.58–309.33 mm SL, Balbina, rio Uatumã, 01°55'21"S 59°28'21"W, 9 Nov 1985, M. Jégu. **Roraima: Caracaraí:** INPA 60152, 6, 190.0–207.7 mm SL, rio Baraúna, lago do Bento, 01°15'34.4"N 60°54'32.4"W, 17 Jan 2021, M. S. Rocha. MUBIO 110, 1, 198.70 mm SL, same collection data as INPA 60152. **Peru: Iquitos: Maynas: Loreto:** ANSP 180369, 4, 67.68–95.01 mm SL (1 x-ray, 71.3 mm SL), (OR366880), rio Nanay, large sandy beach on downstream end of island upstream from Santa Clara, 03°46'56.9"S 73°20'33.3"W, 14 Aug 2003, M. H. Sabaj, N. J. Salcedo & B. Sidlauskas. ANSP 188823, 2, 53.38–62.73 mm SL, (OR366879), rio Nanay, large sandy beach on downstream end of island upstream from Santa Clara, 03°46'56.9"S 73°20'33.3"W, 14 Aug 2003, M. H. Sabaj, N. J. Salcedo & B. Sidlauskas. ANSP 199909, 3, 55.55–61.04 mm SL, rio Nanay, just downstream of sandy beach Las Camelias, 7 km from Iquitos, 03°39'51"S 73°15'01"W, 8 Aug 2010, M. H. Sabaj, B. Sidlauskas, C. A. Phillips, J. Tiemann & E. V. Correa Roldán. CIIAP 401, 1, 206.1 mm SL, rio Pucacuro, tributary of rio Tigre, 03°19'07"S 74°59'05"W, 15 May 2003, J. Ruiz. CIIAP 402, 3, 85.2–8.9 mm SL, rio Nanay, cocha Anguilla, 03°54'34.7"S 73°39'57.7"W, 18 Jul 2018, C. Chavez. CIIAP 403, 5 (3, 97.0–113.0 mm SL), rio Nanay, large sandy beach on downstream end of island upstream from Panpachica, 03°45'07"S 73°17'01"W, 20 Jan 2019, M. Ruiz-Tafur.

Diagnosis. *Myloplus aylan* can be distinguished from all congeners, except *M. schomburgkii* and *M. sauron* n. sp. (described below), by the presence of a vertical black

bar on the flank commonly extending from the dorsal-fin base to the pelvic-fin distal end (*vs.* absence of any conspicuous mark on the flank in the rest of the congeners). The new species can be diagnosed from *M. schomburgkii* and *M. sauron* by the following characters: parietal bone with dorsal surface markedly concave in lateral view (*vs.* straight to slightly concave), 82–95 (mode 84) total perforated scales on lateral line [*vs.* 68–87 (mode 79) in *M. schomburgkii* and 70–82 (mode 78) in *M. sauron*]; 40–41 total vertebrae (*vs.* 36–38), serrae with narrow and long spines (*vs.* short with wide base); 30–39 prepelvic spines (*vs.* 17–29 in *M. schomburgkii* and 20–28 in *M. sauron*); 38–55 (mode 49) total spines [*vs.* 27–41 (mode 33) in *M. schomburgkii* and 29–40 (mode 35) in *M. sauron*). Also, *M. aylan* differs from *M. schomburgkii* and *M. sauron* by presenting, in juveniles and females, anteroposterior decreasing of anal-fin rays length almost uniform, forming broad lobe, occupying half of the anal-fin extension (*vs.* abrupt anteroposterior decreasing of anal-fin rays length, forming narrow falcated anal-fin lobe in juveniles and females, restricted to the anterior half of the fin, not reaching the middle portion of anal-fin base length, with conspicuous dark-red to black pigmentation on the entire anal fin (*vs.* orange to reddish-orange pigmentation along its length, mostly concentrated on anterior rays). Additionally, the new species can be diagnosed from *M. schomburgkii* by presenting anterior ventral-keel spine at the vertical through pectoral-fin origin or anterior to it (*vs.* anterior spine of ventral-keel always inserted posterior to the vertical through pectoral-fin origin); and from *M. sauron* by having greater number of branched dorsal-fin rays (21–25 *vs.* 17–19), wider dorsal-fin base (31.1–37.1% SL *vs.* 25.6–29.1%), shorter distance between last branched dorsal-fin ray and the last branched anal-fin ray [23.4–28.6% SL (mean 25.3%) *vs.* 27.8–32.0% (mean 29.7%)], shorter adipose-fin base [5.0–7.7% SL (mean 6.3%) *vs.* 7.1–9.7% (mean 8.4%)] and greater adipose-fin height (height 0.7–1.1 times in its base *vs.* 0.4–0.6).

Description. Morphometric data presented in Tab. 3. Body compressed, overall rounded to oval, with highest body depth at dorsal-fin origin. Predorsal and postdorsal length almost equivalent. Head rounded, snout length slightly shorter than postorbital distance. Dorsal profile of head convex from mouth to anterior margin of parietal bone, and straight to slightly concave from this point to base of supraoocipital. Dorsal-fin base straight to slightly convex. Last dorsal-fin ray distal end not reaching adipose-fin origin, when adpressed. Distance between dorsal-fin insertion and adipose-fin origin about two times the adipose-fin base. Adipose fin as long as deep, with straight base. Ventral profile of head and body convex from lower lip to anal-fin origin. Anal-fin base slightly convex. Dorsal and ventral profile of caudal peduncle concave.

Mouth terminal. Premaxillary teeth in two rows, outer row with 5*(24) molariform teeth, teeth 1–4 almost equal-sized, tooth 5 smaller, all with sharp, convex edges; inner row with 2*(24) equal-sized teeth with sharp, concave edges; in ventral view, contralateral outer rows forming a V-shaped arch with apex anteriorly pointed; contralateral inner rows forming straight line between the 3rd teeth of outer series, space between rows forming triangular gap. Dentary with 5*(24) molariform teeth, teeth 1–3 substantially bigger than 4–5. Conical symphyseal tooth immediately behind tooth 1 of labial row. Maxilla edentulous.

Scale cycloid, small. Total of perforated scales on lateral line 82(1), 83(3), 84*(5), 85(3), 86(3), 87(1), 89(4), 90(1), 91(1), 94(1), or 95(1). Dorsal-fin base covered by skin

TABLE 3 | Morphometric data of *Myloplus aylan*. Range including the holotype. N = Number of specimens; SD = Standard deviation.

	Holotype	N	Range	Mean	SD
Standard length (mm)	213.0	27	53.4–309.3	–	–
Percentages of standard length					
Body depth	72.4	27	59.2–79.9	73.1	4.7
Head length	29.0	27	26.2–33.7	29.7	2.0
Supraoccipital process	15.8	27	12.1–18.0	14.8	1.4
Predorsal length	61.2	27	57.2–64.5	60.5	1.7
Postdorsal length	55.1	27	51.1–66.5	57.3	3.5
Prepectoral length	29.2	27	28.0–33.8	30.4	1.5
Prepelvic length	60.8	27	57.5–64.8	60.6	1.8
Preanal length	80.1	27	76.3–84.0	79.7	1.8
Dorsal-fin length	23.6	20	22.4–47.7	29.1	8.4
Interdorsal length	9.0	27	7.0–11.8	9.8	1.2
Pectoral-fin length	21.3	27	18.0–23.6	21.3	1.3
Pelvic-fin length	13.8	27	12.8–17.2	16.1	1.5
First anal-fin lobe length	19.2	25	18.6–37.0	25.1	5.0
Second anal-fin lobe length	30.1	3	13.2–14.2	13.2	0.5
Dorsal-fin base length	34.3	27	31.1–37.1	34.5	1.6
Adipose-fin base length	6.4	27	5.0–7.7	6.3	0.7
Anal-fin base length	33.8	27	32.6–40.9	37.0	2.5
Caudal-peduncle depth	10.4	27	8.9–11.5	10.3	0.7
Width of peduncle	4.2	27	2.3–5.8	4.1	1.0
Supraoccipital to dorsal-fin	48.5	27	32.9–48.6	44.5	3.0
Snout to Supraoccipital	29.9	27	27.9–35.6	31.0	2.1
Snout to base of supraocciptal	13.4	21	13.4–18.8	16.4	1.6
Pelvic-anal distance	23.5	27	19.9–24.6	21.9	1.3
Pectoral-pelvic distance	29.8	27	28.0–33.3	30.5	1.3
Dorsal-fin origin to anal-fin origin	74.5	27	64.4–82.2	75.5	4.1
Dorsal-fin end to anal-fin origin	50.9	27	44.6–57.7	53.4	3.1
Dorsal-fin end to anal-fin end	24.5	27	23.4–28.6	25.3	1.3
Percentages of head length					
Head width	17.9	27	13.6–19.4	17.1	1.4
Postorbital distance	41.4	27	25.0–41.4	31.0	4.2
Fourth infraorbital width	20.4	27	7.4–20.4	14.4	3.0
Third infraorbital width	14.9	27	6.9–15.3	11.9	2.6
Cheek gap width	14.6	27	10.8–23.2	15.4	2.3
Interorbital width	58.0	27	38.4–63.6	50.6	6.2
Eye vertical diameter	26.3	27	26.3–40.9	29.6	3.8
Snout length	37.9	27	22.0–38.9	28.7	6.3
Mouth length	43.3	27	19.2–47.9	32.5	8.9
Mouth width	35.3	27	29.2–45.3	34.5	3.8
Percentages of adipose-fin base length					
Adipose-fin length	0.8	21	0.7–1.1	0.8	0.1

flap bearing one or two scale rows. Scale rows between dorsal-fin origin and lateral-line 41(2), 44(2), 45(2), 46(2), 47(2), 49(1), 50(1), 51(1), 55(1), 56(1), 57*(4), 58(2), 60(1), or 61(1). Scale rows between lateral-line and pelvic-fin origin 43(1), 44(1), 45(2), 46(4), 47(3), 48(1), 49(2), 50(3), 51(1), 52*(3), 53(1), 54(1), or 57(1). Adipose-fin base covered by three or four scale rows. Scale rows between the adipose-fin origin and lateral-line 19(2), 20(5), 21(7), 22(8), 23(1), 24(1), or 25*(1). Anal-fin base covered by four or five scales rows. Circumpeduncular scales 34(4), 35(2), 36(5), 37(2), 38*(4), 40(3), 41(2), 42(1), or 44(1).

Dorsal-fin origin slightly anterior to vertical through pelvic-fin origin. Dorsal-fin rays ii, iii*, or iv, 21(1), 22(6), 23*(7), 24(10), or 25(1). Adipose-fin square, length, and depth almost equivalent. Pectoral fin feather-shaped, anterior rays longest. Pectoral-fin rays i*, 13(3), 14(4), 15(6), 16*(12), or 17(2). Anterior pelvic-fin rays longest, not reaching vertical through last spines of serrae. Pelvic-fin rays i,7*(25). Last unbranched anal-fin ray most developed (longest and thicker). Anal-fin rays iii or iv*, 29(1), 30(6), 31*(11), 32(4), 33(2), or 34(1). Caudal-fin forked with almost equal-sized lobes.

Total gill rakers on first branchial arch 27(2), 28(1), 29*(13), 30(5), or 31(2). Upper branch with 12(2), 13*(13), 14(6), or 15(3) rakers; lower branch with 13(1), 14(5), or 15*(17); 1*(23) at cartilage between cerato- and epibranchial.

Osteology. Dorsal profile of neurocranium convex from premaxilla to the posterior margin of frontal bone, markedly concave at parietal, convex from the base to tip of supraoccipital process. Lateral view of supraoccipital triangular. Supraneurals 5(6) or 6(3). Dorsal-fin pterygiophores 23(1), 24(4), or 25(4). First dorsal-fin pterygiophore inserted between neural spines of 9th and 10th(8) or 10th and 11th(1) vertebrae, more developed than remaining pterygiophores, with expanded anterior lamella, and bearing forward-oriented predorsal spine. Predorsal spine somewhat similar to scythe, its dorsal surface smooth; almost completely covered by skin. Anal-fin pterygiophores 31(2), 32(4), or 33(4) (Fig. **S1**).

Total vertebrae 40(8) or 41(1); Weberian apparatus, 4(10); abdominal 18(6) or 19(3) [Predorsal, 5(7) or 6(2); under dorsal-fin 13(8) or 14(1)]; caudal 17(3) or 18(6) [under dorsal-fin 3(4) or 4(5), posterior to dorsal-fin 14(9)]. Anterior spine of ventral keel never reaching vertical through pectoral-fin origin. Long spines, with an almost uniform width throughout its length, with piercing tips. First prepelvic spines covered by skin. Postpelvic spines more developed than prepelvic spines. Total ventral keel spines 38(1), 40(1), 41(1), 46(2), 47(5), 48(3), 49(7), 51(2), 53(1), or 55*(1). Prepelvic spines 30(2), 31(1), 32(4), 33(4), 35(5), or 39*(1); unpaired post-pelvic spines 10(4), 11*(11), or 12(7); and paired spines around anus 4(16), 5*(7), or 6(1).

Coloration in alcohol. Ground coloration yellow to pale brown. Brown pigmentation on dorsal portion of head and body. Middle portion of flanks and belly light yellow. Sclera yellow. Bright yellow pigmentation skirting ventral keel extension. High concentration of melanophores form a broad, vertical brown bar extending from the midpoint of dorsal-fin base to midpoint of pelvic-fin length, wider at lateral line. Pectoral, pelvic and caudal fins yellowish hyaline. Dorsal and anal fins yellow, with conspicuous dark-brown pigmentation most concentrated along base and in extension of anterior rays. Adipose-fin yellow, with dark black outlining on its distal margins (Fig. 2).

Coloration in life. Ground coloration grayish silver. Purplish-silver scales along dorsal region of body, and silvery white scales covering middle portion of flank and belly. Scattered orange-red pigmentation on body, more concentrated on head and pectoral region. Dark vertical bar similar to color in alcohol. Dark olive-yellow pigmentation mostly concentrated on antero-dorsal portion of head. Scattered orangish-red pigmentation on postero-ventral portion of head and pectoral girdle. Sclera white. Paired fins yellowish-hyaline. Basal half of dorsal and caudal fins yellow, followed by white area, and distal ends with dark pigmentation. Adipose fin grayish yellow, with subtle dark margins. Anal fin hyaline with black or dark-red pigmentation throughout (Fig. 3).

Sexual dimorphism. Mature males with two anal-fin lobes; first lobe at anterior rays, less developed; second lobe centered on 13th or 14th branched ray, about twice as long as first lobe. Females and juveniles with single, broad lobe, formed by remarkable prolongation of anterior rays, and occupying more than half of fin (*i.e.*, rays decreasing gradually in length from anteriormost rays to middle rays). Breeding males present black pigmentation throughout body, more conspicuous on head, predorsal region and fins, and dark-red pigmentation mostly concentrated on middle portion of flank. Females present grayish-brown pigmentation on antero-dorsal region of head and predorsal region, all fins grayish-hyaline, except for anal fin (which is dark red to black), red to dark-red pigmentation on middle portion of flank and well-marked vertical bar surrounded by light area. Males also differ from females by presenting long filaments extending dorsal-fin branched rays, and stiff hooks on distal-most lepidotrichia segments of anal-fin branched rays.

FIGURE 3 | *Myloplus aylan*, coloration immediately after capture. Mature female, lago Uauaçu, Purus River basin. Photographed by Lucia Rapp Py-Daniel.

Geographical distribution. *Myloplus aylan* is widespread through Nanay, Tigre (tributary of Marañon), Branco, Juruá, Jutaí, Purus, Madeira, and Uatumã basin, in Peru and Brazil, mostly restricted to the western portion of the Amazon basin. In white water rivers the species is only captured in tributaries with black or clear water (Fig. 4).

Ecological notes. *Myloplus aylan* appears to be more abundant in black water rivers such as the Nanay in Peru, Pitinga, and Jutaí rivers in Brazil. In white water rivers such as the Juruá and Madeira, the species was captured in black water lakes. However, it also occurs in clear water rivers such as Água Boa do Univini and Baraúna, tributaries of the Branco River. White water rivers of Andean origin seem to constitute a chemical barrier for this species, since in the Branco, Juruá and Madeira rivers, the species was captured only in black water lakes of these basins. The same distribution pattern was registered to its congener *M. nigrolineatus* (Ota *et al*., 2020). Ríos-Villamizar *et al*. (2020) classify the black waters of the várzea environments as Intermediate type B, since they present intermediate levels of suspended solids originating from ancient sediments and those recently eroded from the Andes. These characteristics allow the presence of *M. aylan* in Amazonian floodplain environments.

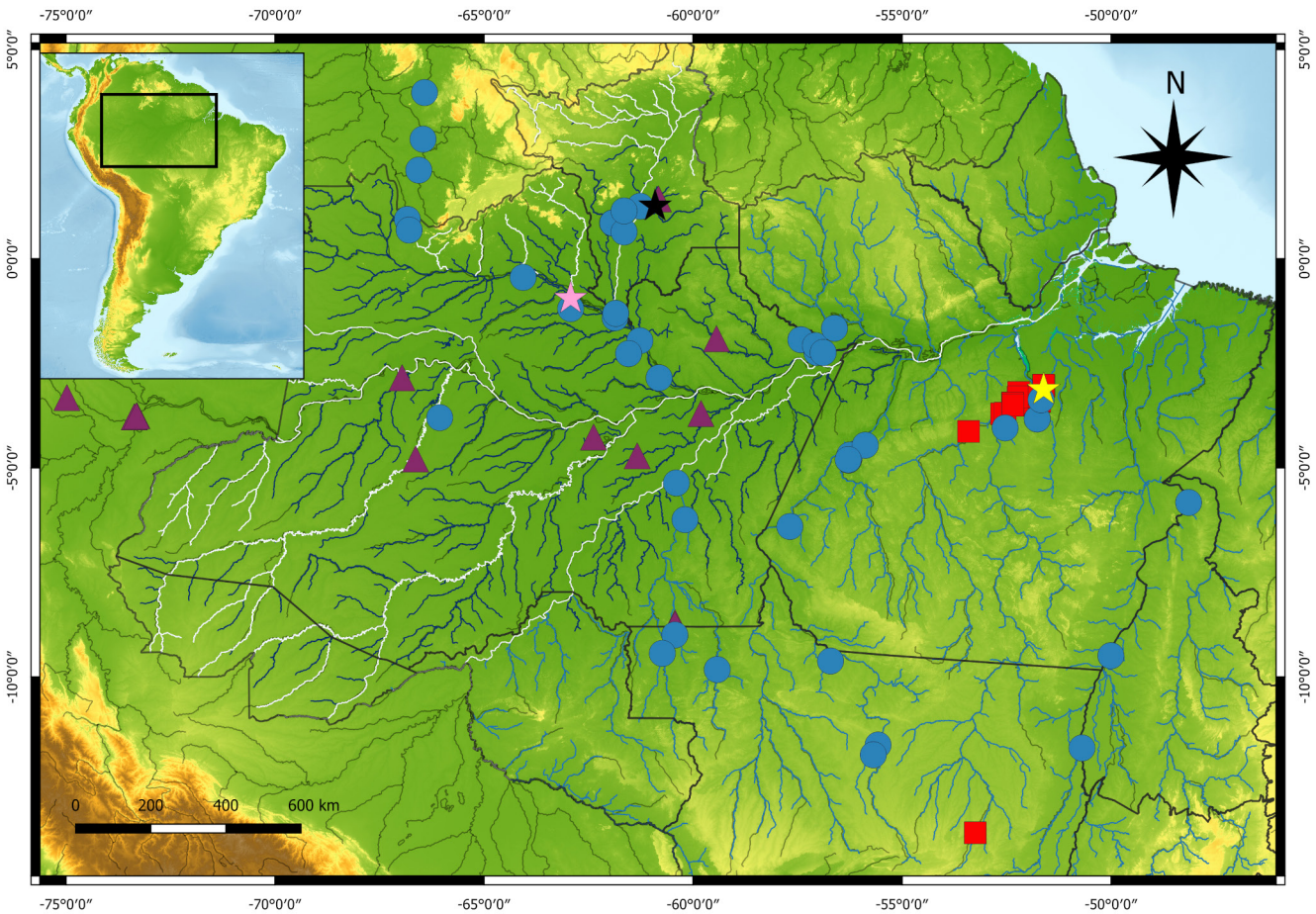

FIGURE 4 | Geographic distribution of *Myloplus schomburgkii* (blue circles; the pink star at rio Negro basin represents the type-locality), *M. sauron* (red squares; the yellow star at rio Xingu basin represents the type-locality) and *M. aylan* (purple triangles; the black star at rio Branco basin represents the type-locality).

Conservation status. This new taxon is threatened by exploitation from commercial fishing (Fig. 5) (upper Solimões River), by pollution, primarily from mining (Branco River) in the environments where it occurs (Nyholt *et al*., 2022; Vasconcellos *et al*., 2022), and by the proposed construction of hydroelectric projects in the region of the upper Solimões River (Winemiller *et al*., 2016; Castello, Macedo, 2016). This species is also exploited to a limited extent by fishing for the ornamental trade, mainly in the upper Solimões region in Peru (García-Dávila *et al*., 2022), where attempts have already been made to reproduce this species in captivity (Murrieta *et al*., 2021), without success. Fish farming of *M. aylan* aims to meet the market demand for ornamental fish and for food consumption, but induced reproduction has not yet been successful. In addition, since 2009 *Myloplus aylan* is considered a species prohibited from extracting and commercializing, unless it comes from management programs in Peru (PERU, 2009). Although many threats are identified in the range of occurrence of *M. aylan*, this species has a wide distribution in western Amazonia. Following the IUCN categories and criteria the species can be categorized as Least Concern (LC) (IUCN Standards and Petitions Subcommittee, 2022).

Etymology. The specific name honors the late Aylan Moraes Andrade, Carine Moraes and Marcelo Andrade's son, born on December 23, 2022, who passed away prematurely on July 6, 2023. Marcelo is one of the authors of this manuscript and this is a tribute to record all the love and dedication of his parents who will never forget him. A noun in apposition.

FIGURE 5 | Sympatric occurrence of *Myloplus schomburgkii* (left) and *M. aylan* (right) in rio Água Boa do Univini, tributary of rio Branco. Both specimens are mature males, the specimens has not being preserved.

Myloplus sauron Pereira, Ota, Machado, Collins, Ândrade, Garcia-Ayala, Jégu, Farias & Hrbek, new species

urn:lsid:zoobank.org:act:ADA03DE2-2F3D-42B0-8860-67BEDC5B7A33

(Figs. 6–8; Tab. 4)

Holotype: INPA 40824, male, 166.39 mm SL, Brazil, Pará, Anapu municipality, rio Xingu, below the Tamaracá waterfall, entrance on the right bank of the river, parallel to BR-230, 03°07'48"S 51°36'50"W, 1 Oct 2013, M. H. Sabaj Pérez, L. M. Sousa, A. Gonçalves, N. K. Lujan, D. B. Fitzgerald & P. M. Ito.

Paratypes. All from Brazil: Pará: rio Xingu basin. Altamira: INPA 4151, 1, 71.64 mm SL, ilha de Babaquara, rio Xingu, 03°18'14"S 52°12'37"W, 4 Oct 1990, L. H. R. Py-Daniel & J. Zuanon. INPA 30884, 2, 56.56–67.06 mm SL, rio Iriri, close to its mouth in rio Xingu, 03°48'54"S 52°37'09"W, 15 Aug 2008, H. Lopez-Fernandez. INPA 31160, 1, 106.63 mm SL, rio Iriri, down stream from mouth of rio Novo, 04°14'14"S 53°24'34"W, 22 Aug 2008, H. Lopez-Fernandez. MZUSP 105723, 1, 110.48 mm SL, rio Xingu, 03°33'43.9"S 51°52'36.9"W, 6 Nov 2000, Eq. Ictiologia UFPA. MNRJ 35028, 1, 158.7 mm SL, rio Curuá, northeast of Castelo dos Sonhos (22 km via BR plus 18 km via secondary road), 08°06'35"S 55°00'58" W, 30 Sep 2008, P. A. Buckup, J. Maldonado & C. Zawadzki. **Anapú:** INPA 40279, 1 (x-ray), 109.97 mm SL, (OR366896), rio Bacajá, 03°31'10"S 51°42'35"W, 15 Sep 2013, M. H. Sabaj. INPA 060148, 1, 138.8 mm SL, rio Xingu, downstream of the Tamaracá waterfall, 03°07'48"S 51°36'50"W, 1 Oct 2013, M. H. Sabaj. MUBIO 109, 1, 163.51 mm SL, rio Xingu, 3.5 km upstream from Praia do Caju, 03°24'29"S 51°43'03"W, 8 Nov 2014, M. H. Sabaj.

FIGURE 6 | *Myloplus sauron*, INPA 40824, holotype, male, 132.8 mm SL, Brazil, Pará, Anapu municipality, rio Xingu, downstream from the Tamaracá waterfall.

Medicilândia: MZUSP 36827, 2 of 4, 60.85–125.06 mm SL, rio Xingu at cachoeira do Espelho, 03°48'00"S 52°31'59.9"W, 23 Oct 1986, P. E. V. Vanzolini. **Senador José Porfírio:** INPA 47142, 4 of 6, 38.6–62.77 mm SL, rio Bacajaí, tributaryof rio Xingu, 03°35'13"S 51°46'00"W, 9 Nov 2014, M. H. Sabaj. **Uruará:** INPA 31820, 1, 110.8 mm SL, Maia community, rio Xingu, canal do Paletó, 03°31'35"S 51°45'04"W, 9 Nov 2008, L. H. R. Py-Daniel. **Mato Grosso: Paranatinga:** LBP 25971, 1, 129.3 mm SL, rio Culuene, 13°50'48"S 53°15'39"W, 25 Jan 2018, N. Falusino Junior, N. Estevão & F. A. Machado.

Non-types. All from Brazil, Pará, rio Xingu basin. Altamira: INPA 4273, 2, ilha de Kaituka, rio Xingu, 03°33'47"S 51°51'20"W, 8 Oct 1990, L. H. R. Py-Daniel & J. Zuanon. INPA 43638, 1, 48.75 mm SL, rio Xingu, 03°33'18"S 52°21'24"W, 18 Mar 2014, I. M. Soares. INPA 47088, 1, rio Xingu, 03°36'34"S 52°20'57"W, 4 Nov 2014, M. H. Sabaj. INPA 47284, 1, 47.38 mm SL, rio Xingu, praia do Caju, 03°02'56"S 51°44'11"W, 7 Nov 2014, I. M. Soares. INPA 47568, 6, ilha de Boa Esperança, rio Xingu, 03°33'44"S 52°21'22"W, 3 Nov 2014, M. H. Sabaj. INPA 47587, 9, rio Xingu, praia Itapuama, 03°36'26"S 52°20'55"W, 3 Nov 2014, M. H. Sabaj. INPA 47793, 5, rio Itatá, tributarity of rio Xingu, 03°37'15"S 51°49'15"W, 10 Nov 2014, M. H. Sabaj. **Anapú:** INPA 4076, 1, 140.7 mm SL, rio Xingu, downstream from Volta Grande, 03°09'04"S 51°36'22"W, 28 Aug 2013, J. Zuanon. INPA 40363, 1, rio Bacajaí, upstream to its mouth in rio Xingu, 03°35'30" S 51°45'56"W, 16 Sep 2013, M. H. Sabaj.

Diagnosis. *Myloplus sauron* can be readily distinguished from all congeners, except *M. schomburgkii* and *M. aylan*, by the presence of a vertical black bar on the flank commonly extending from the dorsal-fin base to the pelvic-fin distal end (*vs.* absence of any conspicuous mark on the flank in the rest of the congeners). The new species can be diagnosed from *M. schomburgkii* and *M. aylan* by having fewer branched dorsal-fin rays (17–19 *vs*. 20–25 in *M. schomburgkii* and 21–25 in *M. aylan*), shorter dorsal-fin base (25.6–29.1% SL *vs.* 29.2–36.7% in *M. schomburgkii* and 31.1–37.1% in *M. aylan*), greater dorsal-fin end to anal-fin end distance [27.8–32.0% SL (mean 29.7%) *vs.* 21.7–28.8% (mean 25.8%) in *M. schomburgkii* and 23.4–28.6% (mean 25.3%) in *M. aylan*], longer adipose-fin base (7.1–9.7% SL (mean 8.4%) *vs*. 4.6–7.2% (mean 6.0%) in *M. schomburgkii* and 5.0–7.7% (mean 6.3%) in *M. aylan*) and lower adipose-fin height (height 0.4–0.6 times in its base, *vs*. 0.5–1.0 in *M. schomburgkii* and 0.7–1.1 in *M. aylan*). Additionally, the new species can be diagnosed from *M. schomburgkii* by presenting anterior ventral-keel spine at the vertical through pectoral-fin origin or anterior to it (*vs.* anterior spine of ventral-keel always inserted posterior to the vertical through pectoral-fin origin). Further, *M. sauron* differs from *M. aylan* by having 70–82 total of perforated scales on lateral line (*vs*. 82–95); fewer prepelvic (20–28 *vs*. 30–39) and total spines (29–40 *vs*. 38–55); 36–37 total vertebrae (*vs*. 40–41); serrae composed by short spines with wide bases (*vs*. long and with narrow bases); dorsal surface of parietal bone straight to slightly concave in lateral view (*vs*. markedly concave) and by abrupt anteroposterior decreasing of anal-fin rays length, forming narrow falcated anal-fin lobe in juveniles and females, restricted to the anterior half of the fin, not reaching the middle portion of anal-fin base length (see Sexual dimorphism) (*vs*. anteroposterior decreasing of anal-fin rays length almost uniform, forming broad lobe, occupying half of the anal-fin extension),

with orange to reddish-orange pigmentation along its length, mostly concentrated on anterior rays (*vs*. conspicuous dark-red to black pigmentation on the entire anal fin).

Description. Morphometric data presented in Tab. 4. Body compressed, overall shape with highest body depth at dorsal-fin origin. Predorsal length slightly longer than postdorsal length. Head rounded, eye at the center of the head. Snout short. Dorsal profile of head convex from mouth to horizontal through dorsal margin of the eye, and straight from this point to base of supraoocipital. Dorsal profile between supraoocipital base and dorsal-fin origin convex. Dorsal-fin base straight to slightly convex. Last dorsal-fin ray distal end not reaching adipose-fin origin when adpressed. Dorsal profile between dorsal-fin insertion and adipose-fin origin straight. Adipose fin longer than deep, with straight base. Dorsal and ventral profile of caudal peduncle concave. Ventral profile of head and body convex from lower lip to anal-fin origin. Anal-fin base straight to slightly convex.

Mouth terminal. Premaxillary teeth in two rows, outer row with 5*(50) molariform teeth, teeth 1–4 almost equal-sized, tooth 5 smaller, all with sharp, convex edges; inner row with 2*(50) equal-sized teeth with sharp, concave edges; in ventral view, contralateral outer rows forming a V-shaped arch with apex anteriorly pointed; contralateral inner rows forming straight line between the 3rd teeth of outer series, space between rows forming triangular gap. Dentary with 5*(50) molariform teeth, teeth 1–3 substantially bigger than 4–5. Conical symphyseal tooth immediately behind tooth 1 of labial row. Maxilla edentulous.

Scales cycloid, small. Total of perforated scales on lateral line 70(1), 72(3), 73(2), 74(1), 75(6), 76(5), 77(5), 78(7), 79(3), 80(1), 81(1), or 82*(4). Dorsal-fin base covered by skin flap bearing one or two scale rows. Scale rows between dorsal-fin origin and lateral line 44(2), 46(2), 47(1), 48(4), 49(3), 50(6), 51(2), 52(3), 53(3), 54(3), 55*(2), 56(2), 57(2), or 59(2). Scale rows between lateral line and pelvic-fin origin 41(1), 42(2), 43(2), 44*(3), 45(5), 46(8), 47(2), 48(3), 49(3), 50(1), 51(4), 54(1), or 55(2). Adipose-fin base covered by five or six scale rows. Scales between adipose-fin origin and lateral line 18(1), 19(1), 21(4), 22(4), 23(5), 24*(14), 25(4), 26(1), or 27(3). Anal-fin base covered by five or six scales rows. Circumpeduncular scales 33(5), 34(5), 35(3), 36(6), 37*(3), 38(5), or 40(3).

Dorsal-fin origin slightly anterior to vertical through pelvic-fin origin. Dorsal-fin rays ii-iii, 17(6), 18*(32), or 19(11). Adipose fin rectangular. Pectoral-fin feather-shaped, anterior rays longest. Pectoral-fin rays i, 14(6), 15*(30), 16(5), or 17(3). Anterior pelvic-fin rays longest, not reaching vertical through last spines of serrae. Pelvic-fin rays i,7*(40). Last unbranched anal-fin ray most developed (longest and thicker). Anal-fin rays iii or iv, 30(1), 31*(6), 32(13), 33(15), 34(1), 35(4), or 36(1). Caudal-fin forked, with almost equal-sized lobes. Total gill rakers on first branchial arch 27(1), 28(6), 29*(12), 30(9), 31(7), or 32(2). Upper branch with 12(1), 13(3), 14*(16), 15(9), or 16(5) rakers; lower branch with 12(1), 13(4), 14*(21), or 15(11) rakers; 1*(38) at cartilage between cerato- and epibranchial.

Osteology. Dorsal profile of neurocranium convex from premaxillae to posterior margin of frontal bone, slightly concave to straight at parietal, convex from base to the tip of supraoccipital process. Lateral view of supraoccipital triangular. Supraneurals 4(1) or 5(9). Dorsal-fin pterygiophores 18(1), 19(1), or 20(8). First dorsal-fin pterygiophore inserted between neural spines of 9th and 10th(7) or 10th and 11th(3) vertebrae, more

TABLE 4 | Morphometric data of *Myloplus sauron*. Range including the holotype. N = Number of specimens; SD = Standard deviation.

	Holotype	N	Range	Mean	SD
Standard length (mm)	166.4	32	38.9–166.4	–	–
Percentages of standard length					
Body depth	66.1	32	66.1–76.1	71.7	2.7
Head length	29.6	32	27.0–32.9	30.0	1.3
Supraoccipital process	18.5	32	13.8–19.4	16.7	1.6
Predorsal length	60.3	32	59.6–66.1	62.4	1.6
Postdorsal length	56.5	32	50.2–58.9	54.4	1.9
Prepectoral length	29.2	32	27.5–34.4	29.9	1.5
Prepelvic length	54.5	32	54.5–61.1	58.3	1.6
Preanal length	73.4	32	73.4–82.5	77.8	2.0
Dorsal-fin length	14.1	25	24.8–69.8	37.4	9.8
Interdorsal length	14.3	32	8.0–14.9	12.3	1.7
Pectoral-fin length	24.2	32	20.6–25.3	22.9	1.0
Pelvic-fin length	16.8	32	14.2–18.3	16.2	1.1
First anal-fin lobe length	22.9	31	20.3–48.7	28.2	5.7
Second anal-fin lobe length	19.4	5	12.7–22.0	19.0	3.3
Dorsal-fin base length	27.0	32	25.6–29.1	27.7	0.9
Adipose-fin base length	8.7	32	7.1–9.7	8.4	0.6
Anal-fin base length	34.8	32	34.8–41.4	38.6	1.4
Caudal-peduncle depth	10.7	32	10.4–11.6	11.0	0.3
Width of peduncle	4.8	32	2.6–5.1	3.6	0.6
Supraoccipital to dorsal-fin	43.9	32	37.9–47.9	43.7	2.5
Snout to Supraoccipital	35.9	32	32.3–42.2	36.8	2.5
Snout to base of supraocciptal	18.5	9	18.1–19.6	18.7	0.5
Pelvic-anal distance	21.9	32	20.7–26.5	22.4	1.6
Pectoral-pelvic distance	26.2	32	24.2–31.1	27.9	1.4
Dorsal-fin origin to anal-fin origin	69.1	32	69.1–79.3	74.7	2.3
Dorsal-fin end to anal-fin origin	51.9	32	51.9–61.3	57.2	2.0
Dorsal-fin end to anal-fin end	30.0	32	27.8–32.0	29.7	1.1
Percentages of head length					
Head width	19.8	32	15.1–22.7	17.7	1.4
Postorbital distance	30.4	32	25.7–32.0	29.0	1.3
Fourth infraorbital width	17.1	32	12.3–21.1	15.8	1.8
Third infraorbital width	19.3	32	12.7–20.1	16.6	2.1
Cheek gap width	16.1	32	12.5–17.1	15.2	1.2
Interorbital width	50.0	32	40.7–53.5	47.3	3.3
Eye vertical diameter	27.7	32	27.5–43.6	33.5	3.4
Snout length	30.4	32	24.5–35.7	32.4	3.5
Mouth length	38.1	31	31.4–42.4	37.1	2.9
Mouth width	36.7	32	30.5–41.8	34.9	2.7
Percentages of adipose-fin base length					
Adipose-fin length	0.5	21	0.4–0.6	0.5	0.1

developed than remaining pterygiophores, with expanded anterior lamella, and bearing a forward-oriented Predorsal-spine. Predorsal spine somewhat similar to scythe, dorsal surface smooth; almost completely covered by skin. Anal-fin pterygiophores 32(1), 33(1), 34(4), 35(3), or 36(1) (Fig. **S2**).

Total vertebrae 36(2) or 37(8); Weberian apparatus, 4(10); abdominal 14(1), 15(7), or 16(2) [pre-dorsal, 5(7) or 6(3); under dorsal-fin 9(2) or 10(8)]; caudal 17(3) or 18(7) [under dorsal-fin 3(4) or 4(6), posterior to dorsal-fin 13(1), 14(7), or 15(2)]. Anteriormost spine of ventral keel never reaching vertical through pectoral-fin origin. Short spines, with wide base and thin piercing tips. First prepelvic spines covered by skin. Postpelvic spines more developed than prepelvic spines. Total ventral keel spines 29(2), 32(4), 33(2), 34(6), 35*(10), 36(5), 37(5), 38(1), 39(1), or 40(1). Prepelvic spines 20(1), 21(3), 22(7), 23(10), 24*(7), 25(5), 26(3), or 28(1); unpaired post-pelvic spines 6(1), 7*(20), 8(11), or 9(4); and paired spines around anus 3(2), 4*(25), or 5(8).

Coloration in alcohol. Ground coloration light grayish brown dorsally, grading to light-yellow ventrally. Narrow, vertical, brown to dark-brown bar on middle of flanks, extending from region near dorsal-fin base to region near ventral-fin distal end, wider on medial portion, narrowing toward its distal ends (Fig. 6). Inconspicuous plumbeous blot on humeral region above lateral line (most common in males). Head brownish gray antero-dorsally and light yellow postero-ventrally. Bright yellow sclera. Pectoral fins dark yellowish hyaline. Pelvic fins light yellow. Dorsal, anal and caudal fins overall yellowish hyaline. Caudal and adipose fins with diffuse brown pigmentation on basal portion. Anal and adipose fins presenting subtle dark line skirting its margins.

Coloration in life. Ground coloration silvery white. Iridescent bluish-green scales on dorsal portion of body, most concentrated above head. Subtle spot of melanophores on humeral region. Scattered patches of light orange-yellow pigmentation around head, covering markedly opercle, interopercle, branchiostegal membrane, and pectoral girdle. Dark vertical bar on flank similar to color in alcohol. Breeding females present a white area around the vertical dark bar. Vertical dark bar inconspicuous in dimorphic males (see Sexual dimorphism). Paired fins light yellowish hyaline. Dorsal and caudal fins overall yellowish orange, with diffuse dark pigmentation on interradial membranes from base to about two thirds of their length, resulting in an orange bar on their margins. Filaments extending dorsal-fin branched rays of breeding males, when present, dark brown. Anal-fin overall orange-yellow and somewhat hyaline, with subtle dark pigmentation along its length in adults; striking orange, with dark distal margins in juvenile (Fig. 7). Adipose-fin orange-yellow and somewhat hyaline.

Sexual dimorphism. Mature males with two anal-fin lobes; first lobe at anterior rays, less developed; second lobe centered on 13th or 14th branched ray, about twice as long as first lobe. Females and juveniles present single falcate lobe, formed by remarkable prolongation of anterior rays. Mature males with long filaments extending dorsal-fin branched rays. Breeding males might present inconspicuous vertical black bar. Breeding females present well-marked bar surrounded by light area. Stiff hooks on distal-most lepidotrichia segment of anal-fin branched rays not observed (Fig. 8).

FIGURE 7 | *Myloplus sauron*, color pattern in life. Young specimen from Xingu River basin, specimen not preserved.

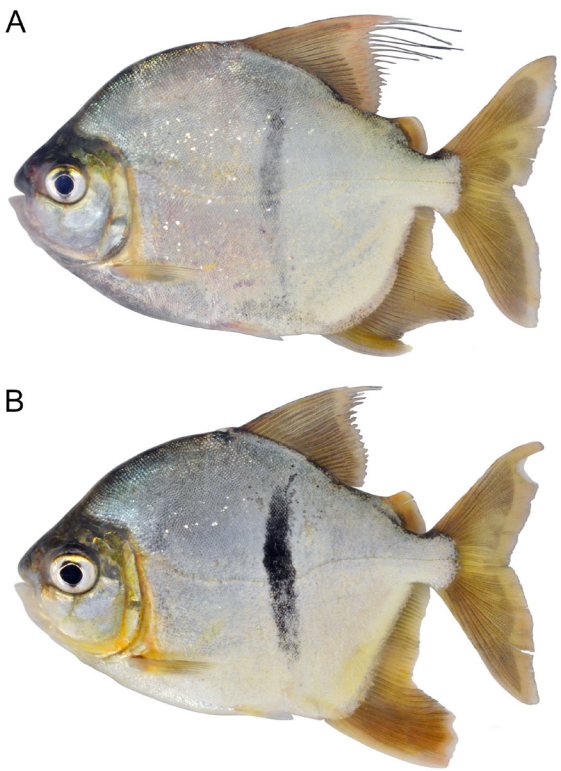

FIGURE 8 | *Myloplus sauron*, coloration immediately after capture. **A.** Male. Notice the faint vertical mark, common during breeding period. **B.** Mature female. Xingu River basin. Photo by M. H. Sabaj.

Geographical distribution. *Myloplus sauron* is known only from the Xingu basin where it is widely distributed, also occurring in its main tributaries such as the Culuene, Iriri, and Bacajá rivers (Fig. 4). However, this species has not yet been recorded below Volta Grande do Xingu rapids.

Ecological notes. *Myloplus sauron* is a rheophilic species only known from the Xingu River basin. The species feeds most on plant material being categorized as herbivore (Andrade *et al*., 2019).

Etymology. The specific name *sauron* alludes to the Eye of Sauron, from J. R. R. Tolkien's "The Lord of the Rings". The elliptical body of *Myloplus sauron*, marked with a vertical, black bar tapering toward both ends, resembles the famous vertical-pupilled eye from the novel. A noun in apposition.

Conservation status. *Myloplus sauron* is a rheophilic species, restricted to the Xingu River basin and, together with its congener *M. schomburgkii,* is commercially exploited to a limited extent by fishing for the ornamental trade (Prang, 2007; Isaac *et al*., 2015). Like most rheophilic fish in this basin, *M. sauron* may be seriously threatened by changes in its habitat caused by alterations in the course of the Xingu River after the construction of the Belo Monte hydroelectric plant, as the flow of the river changed in some stretches (Fitzgerald *et al*., 2017, 2018). However, the species has a wide distribution within this basin, also occurring in tributaries less affected by the Belo Monte dam, such as the Iriri and Culuene rivers. Although some threats are detected in its range, *M. sauron* can be categorized as Least Concern (LC) according to IUCN categories and criteria (IUCN Standards and Petitions Subcommittee, 2022).

Myloplus schomburgkii (Jardine, 1841)

(Figs. 9–14; Tab. 5)

Tetragonopterus schomburgkii Jardine, 1841:243–44 [original description; plate XXII, Schomburk's drawing N. 63; type-locality: "Rio Negro" (Guyana), without a type designation].

Myletes schomburgkii Müller, Troschel, 1844:97 [new combination for *Tetragonopterus schomburgkii* Jardine, 1841]. —Müller, Troschel, 1845:23, 37–38 [redescription based on specimens from "Guyana, Essequibo"]. —Valenciennes, 1850:213–14 [description as a new species similar to *Tetragonopterus schomburgkii*, without considering the new generic arrangement; type-locality: Surinam]. —Steindachner, 1876:134–35 [additional description; comments on sexual dimorphism].

Myletes palometa Valenciennes, 1850:214–15 [original description, type-locality: "Upper Orinoco" (Venezuela)]. —Steindachner, 1876:134–35 [considered a junior synonym of *Myletes schomburgkii*].

Myleus schomburgkii Eigenmann, 1910:443 [listed; new combination for *Tetragonopterus schomburgkii* Jardine, 1841; locality: Essequibo]. —Gosline, 1951:40 [Listed]. —Wallace in Ragazzo, 2002:170–75 [listed; Wallace's plate 29, 96 and 146; locality: Rio Negro (Brazil)].

Mylophus schomburgkii Eigenmann, 1912:391–92 [spelling error; new combination; additional description].

Myloplus schomburgkii Eigenmann, 1915:271 [brief description; plates LVI and LVII, locality: 'Manaos' (=Manaus, Amazonas, Brazil) and Santarem (Pará, Brazil)]. —Norman, 1929:824 [listed; locality: rio Madeira (Amazonas, Brazil)]. —Ohara *et al*., 2017:135 [brief description; photo; locality: Teles Pires (Brazil)]. —

FIGURE 9 | *Myloplus schomburgkii*, INPA 60149, neotype, male, 203.9 mm SL, Brazil, Amazonas, Barcelos municipality, rio Negro.

Machado *et al*., 2018:8 [species delimitation using the mitochondrial gene cytochrome c oxidase subunit I (COI) recovered four lineages identified as *M. schomburgkii*; figs. 3e,f showing morphological variation of individuals from Nhamundá and Tapajós rivers, respectively]. —Kolmann *et al*., 2020:2 [exon-based phylogeny]. —Silvano *et al*., 2020:176 [Listed; brief description; fig. 4.179].

Myleus (*Prosomyleus*) *schomburgkii* Géry, 1977:266 [listed; brief description of the subgenus; photo on page 269, below; locality: Rio Araguaia (Brazil)]. —Géry, 1979:470–71 [description; plate III, above, dentition].

Diagnosis. *Myloplus schomburgkii* can be easily distinguished from all congeners, except *M. aylan* and *M. sauron*, by the presence of a vertical black bar on the flank commonly extending from the dorsal-fin base to the pelvic-fin distal tip (*vs.* absence). The species can be diagnosed from the aforementioned species by presenting anterior spine of ventral-keel posterior to the vertical through pectoral-fin origin (*vs*. anterior ventral-keel spine at the vertical through pectoral-fin origin or anterior to this point). Additionally, *M. schomburgkii* can be distinguished from *M. sauron* by having greater number of branched dorsal-fin rays (20–25 *vs*. 17–19), greater dorsal-fin base (29.7–36.7% SL *vs*. 25.6–29.1%), shorter dorsal-fin end to anal-fin end distance [21.7–28.8% SL (mean 25.8%) *vs.* 27.8–32.0% (mean 29.7%)], and shorter adipose-fin base [4.6–7.2% SL (mean 6.0%) *vs*. 7.1–9.7% (mean 8.4%)]. *Myloplus schomburgkii* can be readily diagnosed from *M. aylan* by possessing dorsal surface of parietal bone straight to slightly concave in lateral view (*vs*. parietal bone markedly concave), 68–87 (mode 79) total perforated lateral-line scales [*vs.* 82–95 (mode 84)], 37–38 total vertebrae (*vs*. 40–41), fewer prepelvic (17–29 *vs*. 30–39) and total ventral-keel spines [27–41 (mode 33) *vs*. 38–55 (mode 49)], and serrae composed by short spines with wide bases (*vs*. long and with narrow bases). Also *M. schomburgkii* differs from *M. aylan* by abrupt anteroposterior decreasing of anal-fin rays length, forming narrow falcated anal-fin lobe in juveniles

and females, restricted to the anterior half of the fin, not reaching the middle portion of anal-fin base length (see Sexual dimorphism) (*vs*. anteroposterior decreasing of anal-fin rays length almost uniform, forming broad lobe, occupying half of the anal-fin extension), with orange to reddish-orange pigmentation along its length, mostly concentrated on anterior rays (*vs*. conspicuous dark-red to black pigmentation on the entire anal fin).

Description. Morphometric data presented in Tab. 5. Body compressed, overall body shape oval, with highest body depth at dorsal-fin origin. Predorsal and postdorsal length almost equivalent. Head rounded, eye at center of the head. Dorsal profile of head convex from mouth to horizontal through dorsal margin of eye, and straight to slightly concave from this point to base of supraoccipital. Dorsal profile between supraoccipital base and dorsal-fin origin convex. Dorsal-fin base slightly convex. Last dorsal-fin ray distal end not reaching adipose-fin origin when adpressed. Dorsal profile between dorsal-fin insertion and adipose-fin origin straight. Adipose-fin deeper than long, with straight base. Ventral profile of head and body convex from lower lip to anal-fin origin. Anal-fin base slightly convex. Dorsal and ventral profile of caudal peduncle concave.

Mouth terminal. Premaxillary teeth in two rows, outer row with 5*(91) molariform teeth, teeth 1–4 almost equal-sized, tooth 5 smaller, all with sharp, convex edges; inner row with 2*(91) equal-sized teeth with sharp, concave edges; in ventral view, contralateral outer rows forming a V-shaped arch with apex anteriorly pointed; contralateral inner rows forming straight line between 3rd tooth of outer series, space between rows forming a triangular gap. Dentary with 5*(91) molariform teeth, teeth 1–3 substantially bigger than 4–5. Conical symphyseal tooth immediately behind tooth 1 of labial row. Maxilla edentulous.

Scales cycloid, small. Perforated scales on lateral line 68(1), 69(2), 71(2), 72(2), 73(5), 74(7), 75(3), 76(7), 77(5), 78(6), 79*(10), 80(4), 81(8), 82(7), 83(4), 84(3), 86(7), or 87(1). Dorsal-fin base covered by skin flap bearing one or two scale rows. Scale rows between dorsal-fin origin and lateral line 38(1), 39(1), 40(2), 41(3), 42(3), 43(6), 44(6), 45*(6), 46(6), 47(7), 48(8), 49(5), 50(2), 51(3), 52(3), 53(5), 54(1), 55(4), 57(2), or 58(1). Scale rows between lateral line and pelvic-fin origin 36(1), 37(3), 38(5), 39(5), 40(10), 41(7), 42*(10), 43(2), 44(4), 45(7), 46(5), 47(2), 48(2), 49(1), 50(1), 51(3), 52(5), 53(1), 54(1), 55(1), or 58(1). Adipose-fin base covered by three or four scale rows. Scale rows between adipose-fin origin and lateral line 15(2), 16(5), 17*(14), 18(18), 19(21), 20(6), 21(10), 22(3), 23(1), or 27(1). Anal-fin base covered by five or six scale rows. Circumpeduncular scales 28(1), 31(3), 32(6), 33(3), 34(13), 35(8), 36(8), 37(12), 38*(10), 39(2), 40(3), or 45(1).

Dorsal-fin origin slightly anterior to vertical through pelvic-fin origin. Dorsal-fin rays ii-iii, 20(11), 21*(36), 22(30), 23(9), 24(3), or 25(1). Adipose-fin square, length and depth almost equivalent. Pectoral fin feather-shaped, anterior rays longest. Pectoral-fin rays i, 12(1), 14(9), 15*(58), 16(21), or 17(7). Anterior pelvic-fin rays longest, not reaching vertical through last spines of serrae. Pelvic-fin rays i, 6(1) or 7*(97). Last unbranched anal-fin ray most developed (longest and thicker). Anal-fin rays iii or iv,

TABLE 5 | Morphometric data of *Myloplus schomburgkii*. Range including the Neotype. N = Number of specimens; SD = Standard deviation.

	Neotype	N	Range	Mean	SD
Standard length (mm)	203.9	100	43.3–236.8	–	–
Percentages of standard length					
Body depth	60.9	99	59.3–78.8	69.0	3.6
Head length	27	100	23.8–34.6	28.7	2.1
Supraoccipital process	17.8	96	12.5–24.5	16.1	2
Predorsal length	54.4	99	54.4–64.4	59.3	1.8
Postdorsal length	56.4	99	49.2–62.4	56.7	2.2
Prepectoral length	28.5	99	24.5–34.1	28.8	2
Prepelvic length	54.6	98	51.7–63.7	58.3	2.3
Preanal length	73.5	99	68.8–82.5	78.5	2.2
Dorsal-fin length	21.8	56	20.3–74.2	35.9	13.3
Interdorsal length	10.6	99	6.2–13.8	11.1	1.7
Pectoral-fin length	20.5	97	17.7–24.1	21.8	1.2
Pelvic-fin length	16.1	97	12.7–18.2	16.4	1.2
First anal-fin lobe length	19.2	84	10.0–39.4	27.6	6.5
Second anal-fin lobe length	19.5	23	11.8–26.5	17.5	4.2
Dorsal-fin base length	35.3	98	29.2–36.7	33.4	1.9
Adipose-fin base length	4.9	97	4.6–7.2	6.0	0.7
Anal-fin base length	34.4	99	31.4–41.3	35.4	1.9
Caudal-peduncle depth	10.4	99	8.0–13.4	10	0.8
Width of peduncle	4.1	98	2.0–5.3	3.9	0.7
Supraoccipital to dorsal-fin	39	97	35.2–47.1	41.4	2.8
Snout to Supraoccipital	34.3	96	15.2–42.8	35	4.2
Snout to base of supraocciptal	16.1	62	15.1–26.8	17.1	2.7
Pelvic-anal distance	20.6	99	18.8–26.1	22.9	1.6
Pectoral-pelvic distance	27	99	24.7–34.4	29.8	1.8
Dorsal-fin origin to anal-fin origin	66.9	98	64.9–81.1	73.1	3.3
Dorsal-fin end to anal-fin origin	46.9	99	45.8–62.0	52.5	3
Dorsal-fin end to anal-fin end	24.4	99	21.7–28.8	25.8	1.5
Percentages of head length					
Head width	17	100	14.0–20.4	17.1	1.1
Postorbital distance	32.2	100	21.1–33.6	28	2.4
Fourth infraorbital width	15.8	98	8.1–18.4	15.2	2
Third infraorbital width	16.4	98	7.8–18.7	14.5	2.2
Cheek gap width	11.8	98	10.3–18.4	13.9	1.9
Interorbital width	50.5	99	34.9–60.8	49	5.6
Eye vertical diameter	32.4	99	26.4–46.1	33.2	4.2
Snout length	36	99	21.0–39.7	32.7	4.7
Mouth length	41.5	99	24.8–43.5	36.3	3.6
Mouth width	33.7	98	24.0–38.0	33.6	2.6
Percentages of adipose-fin base length					
Adipose-fin length	0.7	90	0.5–1.0	0.8	0.1

29(1), 30(1), 31(12), 32(37), 33*(30), 34(4), 35(6), or 36(1). Caudal-fin forked, with almost equal-sized lobes. Total gill rakers on first branchial arch 27(9), 28*(22), 29(19), 30(9) or 31(6). Upper branch with 12(12), 13(32), 14*(15) or 15(7) rakers; lower branch with 13*(7), 14(26), 15(32), or 16(1) rakers; 1*(66) raker at cartilage between cerato- and epibranchial.

Osteology. Dorsal profile of neurocranium convex from premaxilla to posterior margin of frontal bone, slightly concave to straight at parietal, convex from base to tip of supraoccipital process. Lateral view of supraoccipital triangular. Supraneurals 5(15). Dorsal-fin pterygiophores 22(3), 23(5), 24(4) or 25(2). First dorsal-fin pterygiophore inserted between neural spines of 8th and 9th(11) or 9th and 10th(4) vertebrae, more developed than remaining pterygiophores, with expanded anterior lamella, and bearing forward-oriented predorsal spine. Predorsal spine somewhat similar to scythe, dorsal surface smooth; almost completely covered by skin. Anal-fin pterygiophores 30(1), 31(1), 32(3), 33(6), or 34(1) (Fig. **S3**).

Total vertebrae 37(12) or 38(1); Weberian apparatus 4(15); abdominal 15(3), 16(9), or 17(1) [pre-dorsal, 4(11) or 5(4); under dorsal-fin 11(5), 12(7), or 13(1)]; caudal 16(1), 17(8) or 18(4) [under dorsal-fin 3(5), 4(7), or 5(1); posterior to dorsal-fin 13(6), or 14(7)]. Anteriormost spine of ventral keel never reaching vertical through pectoral-fin origin. Spines overall thin, with wide base and piercing tips. First prepelvic spines covered by skin. Post pelvic spines more developed than prepelvic spines. Total ventral keel spines 29(3), 30(2), 31(5), 32(9), 33(13), 34(12), 35*(13), 36(4), 37(2), 38(2), 39(2), or 40(2). Composed by prepelvic spines 17(2), 18(3), 19(14), 20(9), 21(14), 22(9), 23(7), 24*(4), 25(2), 26(4), 27(2), or 29(1); postpelvic spines 7(11), 8*(34), or 9(26); and paired spines around anus 3*(6), 4(40), or 5(24).

Coloration in alcohol. Ground coloration light brown dorsally, grading to light-yellow ventrally. Sclera light yellow. Great concentration of melanophores form a wide, well-marked vertical bar extending from region near dorsal-fin base to region near ventral-fin distal end. Numerous scattered, irregular, light brown to dark-brown blots of variable sizes on the entire body including head and fins, mostly concentrated on dorsal regions of body and head. Paired fins yellowish hyaline. Dorsal, anal, and caudal fins yellowish hyaline with inconspicuous dark pigmentation along its distal margins. Adipose fin yellow to light brown (Fig. 9).

Coloration in life. Based on the Neotype and similar specimens (Fig. 10). Ground coloration grayish silver. Whitish-silver iridescent scales on dorsal region of body. Vertical dark bar and scattered dark blots similar of color in alcohol. Scattered striking red pigmentation mostly concentrated along anterior portion of body (including head), becoming less perceptible at posterior portion (see Sexual dimorphism). Different colors of blots confer a rust appearance to specimens. White sclera, in occasional specimens presenting subtle orange-red pigmentation. Paired fins grayish hyaline, with dark pigmentation concentrated along anterior rays. Dorsal, anal, and caudal fins grayish hyaline, with diffuse dark pigmentation along interradial membranes. Adipose fin grayish brown.

FIGURE 10 | *Myloplus schomburgkii*, color pattern immediately after capture. **A.** INPA 60149, neotype, 203.9 mm SL, male, with second lobe well developed and remarkable breeding coloration. **B.** INPA 52507, 197.1 mm SL, female. Both from Amazonas, Barcelos municipality, rio Negro.

Sexual dimorphism. Mature males with two anal-fin lobes; first lobe at anterior rays, less developed; second lobe centered on 12th or 14th branched ray, about twice as long as first lobe (Fig. 10A). Females and juveniles present single falcate lobe, formed by remarkable prolongation of anterior rays (Fig. 10B). On breeding period male specimens present abundant, striking red pigmentation covering most of head and anterior portion of body, spreading through posterior portion less conspicuously, as scattered spots. Females present orangish-red spots of variable sizes, also more concentrated on head

and anterior portion of body, but not covering great uninterrupted areas. Though both sexes present scattered, irregular, dark brown to black blots of variable sizes on entire body including head and fins, in females those are less evident. Males present filaments extending dorsal-fin branched rays, and stiff hooks on distal-most lepidotrichia segment of anal-fin branched rays.

Geographical distribution. *Myloplus schomburgkii* is widespread through the Orinoco and Amazon river basins, occurring in the Casiquiare, Branco, Negro, Aripuanã, Nhamundá, Uatumã, Pitinga, Trombetas, Tapajós, Teles Pires, Xingu and Araguaia, rivers in Venezuela and Brazil. In white water river basins, the species is only captured in tributaries with black or clear water (Fig. 4).

Geographic variation. The species displays three different, well recognizable types of vertical bar on the flanks, which vary in length and shape according to the area of occurrence. In the left bank tributaries of the Amazon River, draining the Guiana shield, the specimens present a well-developed bar (Fig. 11A), extending from near the dorsal-fin base to near the pelvic-fin insertion, always conspicuous below lateral line, presenting regular width throughout its length. Conversely, specimens collected on the right bank of the Amazon River basin (Tapajós, Teles Pires, Xingu and Tocantins rivers) present a shorter bar. Specimens from Teles Pires river basin have the portion of the midlateral bar immediately dorsal to the lateral line much more conspicuous, with the appearance of a well-defined, round to vertically oval black spot (Fig. 12); in some specimens, the portion of the midlateral bar ventral to the lateral line is very faint, although still perceptible; in other specimens, it is unrecognizable (Fig. 13). Besides these two different well-defined types of bars, an intermediary type is observed in specimens from Tapajós, Xingu and Tocantins river basins, in which the midlateral bar is much more conspicuous immediately dorsal to lateral line, with rectangular appearance, while the portion ventral to lateral line is very faint (Fig. 11B). Although these populations present this color pattern variation, they were recovered as a single lineage in molecular analysis, with low intraspecific variance.

Ecological notes. The species inhabits slow-flowing environments in clear and black water rivers that drain the Guiana and Brazilian Shields. It feeds mainly on aquatic plants (Goulding, 1980), but aquatic insects are also part of its diet (Dary *et al*., 2017). Although it has been described for the Rio Negro basin, a river with acidic waters (Sioli, 1984; Venticinque *et al*., 2016), *M. schomburgkii* occurs mainly in rivers with clear waters that have low concentrations of sediments and humic compounds (Sioli, 1984; Ríos-Villamizar *et al*., 2014; Venticinque *et al*., 2016) such as the Aripuanã, Branco, Nhamundá, Trombetas, Tapajós and Tocantins-Araguaia rivers. White water river basins of Andean origin seem to constitute a chemical barrier for this species, since in the Branco, Purus and Madeira rivers, the species was captured only in black water lakes of these basins. The same distribution pattern was registered to its congener *M. nigrolineatus* (Ota *et al*., 2020). Ríos-Villamizar *et al*. (2020) classify the black waters of the várzea environments as Intermediate type B, since they present intermediate levels of suspended solids originating from ancient sediments and those recently eroded from the Andes. These characteristics allow the presence of *M. schomburgkii* in Amazonian floodplain environments.

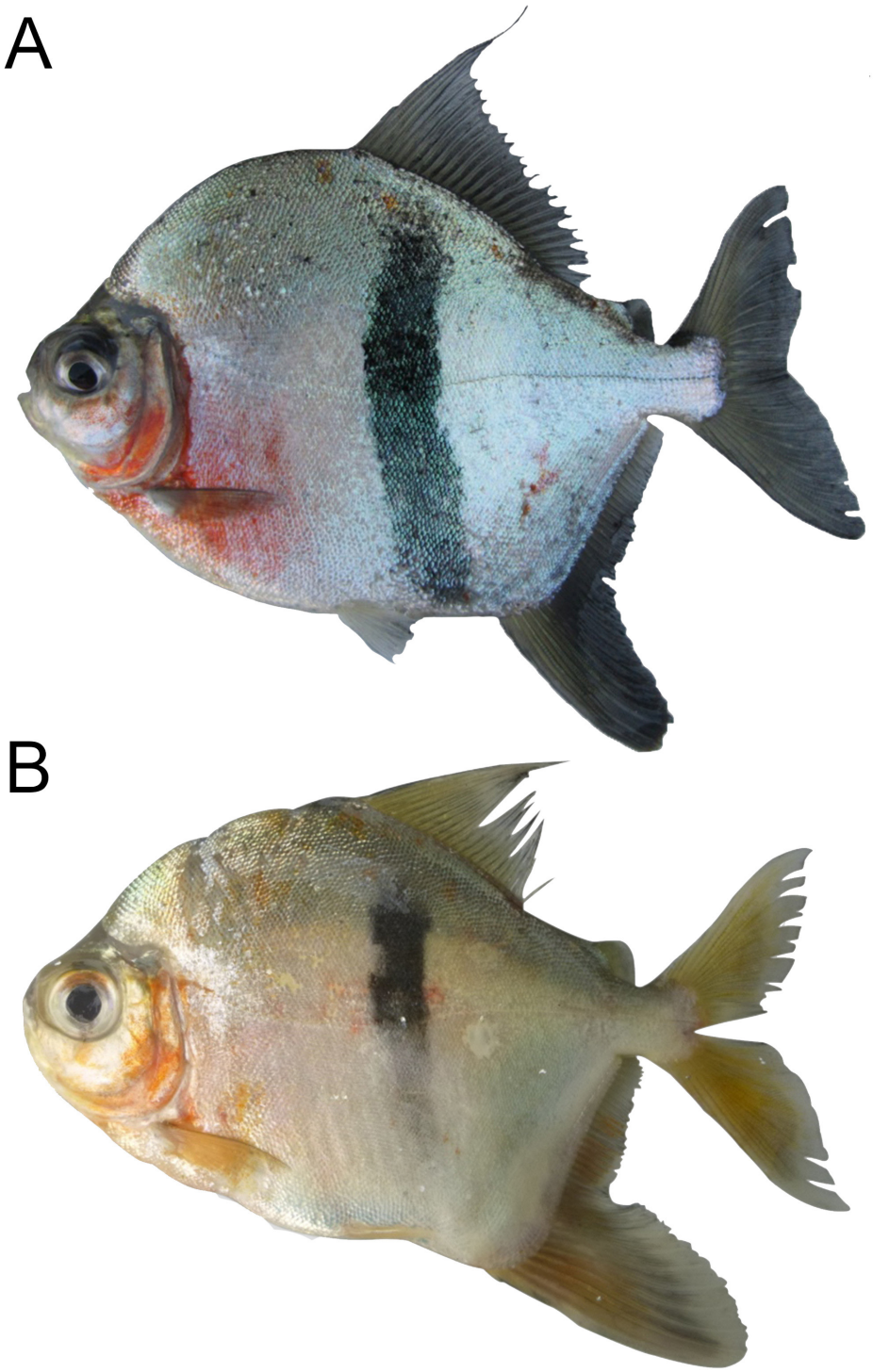

FIGURE 11 | Geographic variation in *Myloplus schomburgkii*. **A.** Roraima, Caracaraí municipality, rio Água Boa do Univiní. **B.** Tapajós River basin. Both recently collected, females, not preserved. Notice, in **A**, the vertical bar conspicuous across the flank, while in **B** the bar is conspicuous only dorsally to the lateral line.

FIGURE 12 | Geographic variation in *Myloplus schomburgkii*, 202.4 mm SL. Teles Pires River basin. Notice the oval mark on the flank, instead of a vertical bar.

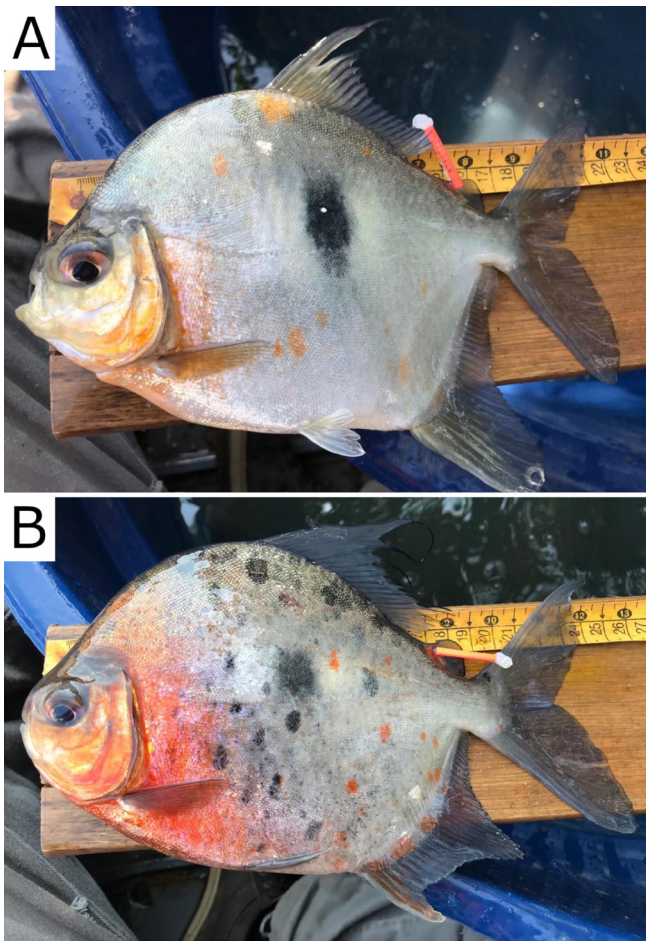

FIGURE 13 | Geographic variation in *Myloplus schomburgkii*. Both from the Teles Pires River basin, immediately after capture. **A.** Female. **B.** Male. Notice the oval mark on the flank, instead of a vertical bar. Photographed by Renan Condé Pires, not preserved.

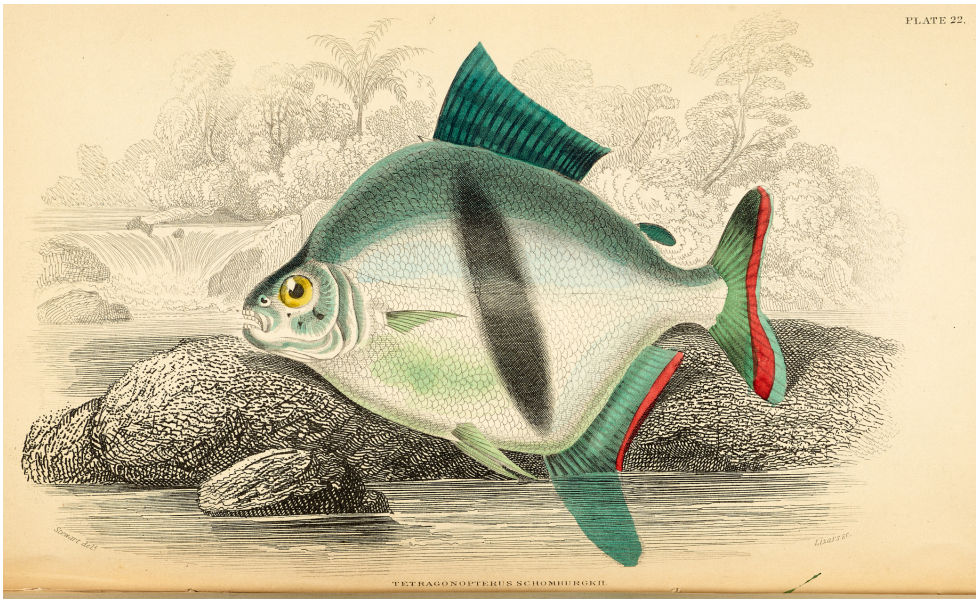

FIGURE 14 | Illustration of a female from rio Negro basin, provided by Robert H. Schomburgk, in which Jardine in Schomburgk (1841, plate 22) based the original description of *Tetragonopterus schomburgkii*.

Etymology. *Myloplus schomburgkii* was described in honor of Robert H. Schomburgk, who, during an expedition to English Guyana, collected individuals of the species, took notes, and illustrated (Fig. 14) the specimen used by Jardine (1841) to describe the new species. A genitive noun.

Remarks. Taxonomic history. Jardine (1841) described several species of Neotropical fishes based on illustrations and commentaries provided by Robert H. Schomburgk from his expedition to Guyana, French Guyana, Surinam, and northern Brazil. Among those species, Jardine (1841) described *Tetragonopterus schomburgkii* (=*Myloplus schomburgkii*) based on the plate XXII (illustration 68 of Schomburgk; Fig. 14), from "Rio Negro", without mentioning the precise type-locality or the existence of a preserved type specimen. Although Jardine (1841) did not designate a holotype, according to Art. 73.1.2. of ICZN (International Commission on Zoological Nomenclature) the holotype was fixed by monotypy, once it is possible to deduce that the author based the description on a single specimen. Furthermore, Art. 73.1.4. states that the "Designation of an illustration of a single specimen as a holotype is to be treated as designation of the specimen illustrated; the fact that the specimen no longer exists or cannot be traced does not of itself invalidate the designation". Thus, the specimen on which Schomburgk based his illustration (see Jardine, 1841: plate XXII) and meristic data is the holotype.

Müller, Troschel (1844:97) placed *Tetragonopterus schomburgkii* in *Myletes*. Subsequently, Müller, Troschel (1845:37–38) provided a complementary description based on a specimen from "Guiana, in Essequibo" collected by Richard Schomburgk (Robert Schomburgk's brother) and deposited in the Zoological Museum of Berlin (ZMB). Zarske (2012) found at ZMB three lots identified as *Myletes schomburgkii*: ZMB 3638, from Guyana collected by Robert Schomburgk, and ZMB 3639–3640 from Surinam, collected by Stegelich. Jégu, Santos (2002) identified the specimens of lots ZMB 3639 and 3640 as *Myleus setiger* Müller & Troschel, 1844 in the species

redescription, based on teeth arrangement (two premaxillary teeth rows in contact) and on color pattern, with no evidence of a vertical dark bar on the flank, the main diagnostic feature of *M. schomburgkii*. But the authors did not consider them as type-series of *Myleus setiger* because they were collected in Surinam, and its type-locality is Guyana. As Zarske (2012) also provided a figure, x-ray, and a brief description of ZMB 3639, we corroborate here the identification of Jégu, Santos (2002). Another important fact is that they were collected by Stegelich, could not correspond to the specimens used by Müller, Troschel (1845) to redescribe *M. schomburgkii*.

Eigenmann, during a visit to ZMB in 1910, identified ZMB 3638 as *Myleus setiger*, and Zarske (2012) suggested it could be *Myleus planquettei*. However, Jégu, Santos (2002) mentioned the presence of a gap between the two premaxillary teeth rows, and at the symphysis in this specimen, a character currently used to diagnose *Myloplus* from *Myleus*. The authors could not identify this specimen at a specific level. The specimen cataloged as ZMB 3638 is a female (184 mm SL), with 25 total dorsal-fin rays; 39 total anal-fin rays (MJ, pers. obs.). Although it could represent the specimen used by Müller, Troschel (1845) to redescribe *M. schomburgkii*, it does not fit the original description and is not the holotype of *Tetragonopterus schomburgkii* Jardine, 1841, once it was collected in Guyana (*vs*. *T. schomburgkii* type-locality Rio Negro). Therefore, none of the lots deposited in ZMB could represent the holotype, and the designation of a neotype is necessary (see designation of neotype below).

Valenciennes (1850), in a comprehensive study of the ichthyofauna from Surinam, described *Myletes schomburgkii* based on a specimen collected by H. H. Dieperink (erroneously spelled Diepering) and deposited in Rijksmuseum van Natuurlijke Historie in Leiden by C. J. Temminck (the director of the Museum). Posteriorly, this material was donated to MNHN (Muséum National d'Histoire Naturelle), in Paris (Boeseman, 1972). This lot was not found (MJ, pers. obs). On the other hand, the possibility of ZMB 3638 and 3639 being syntypes of *Myletes schomburgkii*, raised by Fricke *et al*. (2023), certainly can be ruled out. In the description, despite mentioning it as a new species, Valenciennes (1850:212–13) highlighted that the new species "seems to be an extremely close species to *Tetragonopterus schomburgkii*"; and cited parts of the original description of *T. schomburgkii*, without providing a diagnosis between the two species.

Subsequently, Valenciennes (1850:214–15) described *Myletes palometa* from "upper Orinoco" River, based on the observations made by Mr. Humboldt. He stated that *M. palometa* had a color pattern very similar to *T. schomburgkii* but described it as a different species because it was collected from another river basin. He did not establish a type specimen for *M. palometa*. Finally, in the same manuscript, Valenciennes (1850:215–16) described *Myletes divaricatus*, a species with similar body shape, but with a second anal-fin lobe, indicating it was a male. The author did not mention the presence of a vertical bar on the middle of the flanks.

Kner (1860:23–24) examined specimens from Rio Branco (Brazil) that had a second anal-fin lobe. However, they had the typical color pattern of *T. schomburgkii* (*i.e*., dark vertical bar on the middle of the flank). Thus, the author suggested that the second anal-fin lobe might consist of a secondary sexual character. By the analysis of the gonads, Steindachner (1876:134–35) confirmed that the presence of a second anal-fin lobe is present exclusively in males, corroborating this feature as a secondary sexual character of *Myletes schomburgkii*. Furthermore, he considered *Myletes schomburgkii* the senior

synonym of *Myletes palometa* Valenciennes, 1850 and *M. divaricatus*. Posteriorly, *M. divaricatus* was considered a junior synonym of *Myleus setiger* by Jégu, Santos (2002:51, fig. 10a), and *M. palometa* a junior synonym of *T. schomburgkii* by Jégu (2003). According to our molecular results, specimens from Rio Orinoco were recovered within the *M. schomburgkii* clade, corroborating the synonymy proposed by Steindachner (1876) and Jégu (2003).

Neotype designation. We provide the designation of a neotype, to better define *Myloplus schomburgkii*, and set a precise type-locality to facilitate the comparison among the congeners described herein [See taxonomic history for explanation about lots ZMB 3638–3939 pointed by Fricke *et al*., 2023 as possible syntypes of *Myletes schomburgkii*]. Although the specimen illustrated was a female, considering the presence of solely an anterior lobe on anal fin (*vs*. two lobes in males), we chose a male specimen as the neotype, considering it was better preserved and exhibited secondary dimorphism of the species. We also restricted the species type-locality to Rio Negro, Barcelos (INPA 60149) (Fig. 9).

In the original description, Jardine (1841) provided information on general morphology of the body; color pattern, highlighting the presence of a vertical dark bar on the middle of flank; and counts of total fin rays (dorsal-fin rays 25; pectoral-fin rays 15; total pelvic-fin rays 8; total anal-fin rays 39; caudal-fin rays 27); branchiostegal rays (4); ribs (13); and vertebrae (34). Even though the remarkable color pattern of the species was considered until now an autapomorphy, herein we describe two additional species previously identified as *M. schomburgkii*, that also present a vertical mark on the middle of the flank. Thus, a brief commentary is necessary to explain how we deduced which specimens were conspecific with the holotype and how we based our choice of the neotype.

Myloplus schomburgkii can be promptly distinguished from *M. aylan* by the anal-fin lobe extension, dark vertical bar shape, and total vertebrae counts provided by Jardine (1841). In *M. aylan* the anteriormost anal-fin rays length decreases gradually, forming a broad lobe, occupying half of the anal-fin base length (*vs*. anal-fin rays length decreasing abruptly, forming a narrow falcated anal-fin lobe in juveniles and females, restricted to the anterior third of the fin or slightly posterior to that point, not reaching the middle portion of anal-fin base in *M. schomburgkii*). The figure of the holotype in the original description (Jardine, 1841: plate XXII) clearly illustrates the narrow anal-fin lobe. The vertical dark bar is also different in the two congeners, with a uniform width in *M. schomburgkii* and wider in the central portion in *M. aylan*. Furthermore, the original description mentions a total of 34 vertebrae (without Weberian apparatus), whereas *M. aylan* has at least 36 total vertebrae (without Weberian apparatus).

The *Myloplus sauron* is from Xingu River basin and has a color pattern that resembles Schomburgk's illustration (*i.e*., bluish-green scales mostly concentrated at dorsal region of the body and vertical mark on the flanks tapering toward both ends). Nonetheless, Jardine cited the presence of 25 total dorsal-fin rays, and the greatest count known for *M. sauron* is 22. *Myloplus sauron* also differs from the specimen illustrated by having a long adipose-fin base (*vs*. short). Finally, *M. sauron* is restricted to Xingu River basin and its occurrence at Negro River basin is unlikely.

In addition, in the species delimitation analysis, the species were recovered as distinct lineages in all methods. The interspecific genetic distance between *M. schomburgkii* and *M. aylan* was 7.9%; and *M. schomburgkii* and *M. sauron* was 9.7%. For further detailed comparison between *M. schomburgkii* and all congeners see Diagnosis and Molecular Results.

Material examined. Neotype (Present designation). INPA 60149, male, 203.9 mm SL, CTGA 12333 (GenBank accession MG752391.1), Brazil, Amazonas, Barcelos municipality, rio Negro, 00°56'56.6"S 62°55'44.3"W, 20 Feb 2013, V. N. Machado. **Brazil: Amazonas: Barcelos:** INPA 52507, 2, 170.8–197.1 mm SL, CTGA 12274 (MG752389), 12335 (MG752393), rio Negro, 00°56'56.6"S 62°55'44.3"W, 20 Feb 2013, V. N. Machado. MZUSP 91456, 1, 208.16 mm SL, Tapera community, rio Negro, 00°12'00"N 64°04'00"W, 1 Nov 1972, Expedição Permanente à Amazônia. **Apuí:** INPA 33610, 76.0 mm SL (x-ray), Amazonas, rio Guariba at Reserva Extrativista do Guariba, 08°42'42"S 60°25'53"W, 14 Nov 2008, W. S. Pedroza, W. Ohara, F. R. Ribeiro & T. F. Teixeira. INPA 36251, 197.5 mm SL, Amazonas, rio Guariba at Reserva Extrativista do Guariba, 08°42'42"S 60°25'53"W, 7 Nov 2008, W. S. Pedroza, W. Ohara, F. R. Ribeiro & T. F. Teixeira. **Nhamundá:** INPA 46309, 2, 162.8–175.3 mm SL, CTGA 14526 (MG752395), 14527 (MG752396), rio Paracatu, tributary of rio Nhamundá, 01°59'51"S 57°2'12"W, 10 Nov 2013, V. N. Machado & R. A. Collins. INPA 46311, 1, 62.9 mm SL, CTGA 14479 (MG752394), rio Nhamundá, 01°41'26.9"N 57°25'19.9"W, 11 Nov 2013, V. N. Machado. INPA 46312, 2, 138.5–173.7 mm SL, rio Nhamundá, 01°49'54.9"S 57°04'23.9"W, 12 Nov 2013, V. N. Machado & R. A. Collins. **Novo Airão:** INPA 30716, 1, 144.4 mm SL, rio Carabinani, 02°01'24.9"S 61°32'35.9"W, 25 Oct 2004, L. N. Carvalho. INPA 39024, 1, 170.5 mm SL, rio Jauaperi, close to its mouth in rio Negro, 01°42'56"S 61°16'19.9"W, 20 Sep 2011, R. P. Ota. INPA 46062, 3, 151.7–183.4 mm SL, rio Negro, Arquipélago de Anavilhanas, 02°36'10"S 60°48'46"W, 7 Nov 1996, V. Garcia. **Novo Aripuanã:** INPA 35586, 2, 194.6–223.7 mm SL, São Miguel community, rio Aripuanã, 05°59'39.9"S 60°11'35.9"W, 12 Set 2004, L. H. R. Py-Daniel. **Presidente Figueiredo:** INPA 22192, 1, 236.8 mm SL, vila de Balbina, rio Uatumã, 01°55'21"S 59°28'21"W, 9 Nov 1985, M. Jégu. INPA 22193, 1, 214.81 mm SL, rio Uatumã, igarapé do Arraia, 01°54'31"S 59°28'18"W, 1 Nov 1985, M. Jégu. INPA 46055, 3, 150–203.9 mm SL, vila de Balbina, rio Pitinga at Cachoeira 40 ilhas, 01°08'59.9"S 59°34'59.9"W, 14 Oct 1996, V. Garcia. **São Sebastião do Uatumã:** INPA 46059, 3 of 4, 207.83–178.24 mm SL, Santa Maria community, rio Capucapu, close to its mouth in rio Jatapú, cachoeira das Garças, 01°42'59"S 58°34'58"W, 25 Sep 1995, V. Garcia. **Mato Grosso: Paranaíta:** INPA 44790, 1, 66.7 mm SL, rio Teles Pires 09°30'33"S 56°42'29.9"W, 9 Oct 209, R. R. de Oliveira. INPA 45456, 5, 58.1–107.4 mm SL, rio Teles Pires, Inventário CHTP, 09°22'29"S 56°42'43"W, 15 Dec 2021, Solange, Reginaldo & Rosalvo. INPA 59651, 1, 156.8 mm SL, rio Teles Pires, 09°22'30"S 56°42'43"W, L. N. Carvalho. MZUSP 99863, 5 of 13, 46.2–45.7 mm SL, rio Teles Pires, 09°18'42"S 56°46'46.9"W, 9 Mar 2008, L. Netto-Ferreira. **Carlinda:** MZUSP 68215, 1, 93.3 mm SL, rio Teles Pires, 09°59'25"S 55°33'48"W, 29 Sep 2007, F. A. Machado. **Paranatinga:** MZUSP 94072, 5, 110.38–134.54 mm SL, rio Culuene at cachoeira do Adelino, 13°53'55'S 53°19'17"W, 20 May 2007, F. C. T. Lima, F. A. Machado & J. Birindelli. MZUSP 98124, 3, 121.34–

144.82 mm SL, rio Culuene, 13°49'59.9"S 53°15'00"W, 2 Oct 2007, F. C. T. Lima, F. A. Machado, A. C. Ribeiro & C. L. R. Moreira. **Peixoto de Azevedo:** MZUSP 97639, 5, 152.7–200.9 mm SL, (OR366886), rio Peixoto de Azevedo, tributary of rio Teles Pires, 10°17'13.9"S 54°50'57"W, 17 Oct 2007, J. Birindelli, L. Netto-Ferreira, M. H. Sabaj & N. Lujan. **Pará: Oriximiná:** MZUSP 15656, 1, 208.9 mm SL, rio Trombetas at Reserva Biológica do Trombetas, 01°25'00"S 56° 37'00"W, 23 Jul 1979, M. Goulding. **Roraima: Atauba:** INPA 46280, 2, 152.3–198.8 mm SL, CTGA 12199 (MG752387), 12200 (MG752388), left bank of rio Branco, 01°03'38"S 61°51'00"W, 10 Dec 2013, V. N. Machado & R. A. Collins. **Caracaraí:** INPA 23398, 1, 174.53 mm SL, CTGA 14611 (MG752398), rio Capivara, tributary of rio Branco, 01°06'00"N 61°55'41"W, 10 Dec 2013. V. N. Machado. MZUSP 79209, 2, 131.6–168.7 mm SL, rio Branco, 01°30'00"N 61°16'00"W, 28 Oct 1979, M. Goulding. MZUSP 79210, 2, 161.7–194.7 mm SL, rio Branco, 01°10'00"S 61°52'00"W, 9 May 1979, M. Goulding. **Venezuela:** ANSP 192193, 1, 110.7 mm SL, caño Yurebita, tributaryof rio Ventuari, 04°13'07.64"N 66°25'25.5"W, 15 Apr 2010, N. K. Lujan, J. Birindelli & V. Meza.

Molecular differentiation. We obtained sequence data for representatives of 10 of the 12 recognized species of *Myloplus*: *M. arnoldi*, *M. asterias*, *M. levis* (Eigenmann & McAtee, 1907), *M. lobatus*, *M. lucienae*, *M. rubripinnis*, *M. schomburgkii*, *M. tiete* (Eigenmann & Norris, 1900), *M. nigrolineatus* and *M. zorroi* Andrade, Jégu & Giarrizzo, 2016. No tissues or sequences of *M. tumukumak* Andrade, Jégu & Gama, 2018 and *M. torquatus* were available. Nineteen additional nominal Myleini species were also used in the analysis (Fig. 15). A total of 89 sequences initially identified as "*Myloplus schomburgkii*" were obtained, with 40 of these newly generated. These "*M. schomburgkii*" sequences represent 36 haplotypes and 32 unique localities from six major tributaries of the Amazon basin in Brazil (Negro, Branco, Nhamundá, Madeira, Tapajós, Xingu), as well as the Nanay River in Peru, Orinoco basin, and Tocantins-Araguaia system.

The full nucleotide dataset represented 564 sequences of a median sequence length of 612 bp (range 312–621 bp). After dereplication, 209 sequences of length 621 bp remained (range 405–621 bp). Species discovery using mPTP on the maximum clade credibility consensus of MrBayes trees partitioned the haplotype dataset into 48 putative species clusters (Fig. 15). Within "*M. schomburgkii*" a total of six geographically-structured species clusters were estimated, comprising: a taxon from the Xingu River corresponding to *M. sauron* (BPP = 0.97); a taxon from the upper Amazon, Madeira and Branco rivers corresponding to *M. aylan* (BPP = 0.96); *M. schomburgkii* from Brazilian Shield rivers including Lower Xingu, Tapajós and Araguaia (BPP = 0.16); *M. schomburgkii* from Guiana Shield rivers including Negro, Branco and Nhamundá (BPP = 0.26); *M. schomburgkii* from Orinoco and Casiquiare rivers (BPP = 0.32); and *M. schomburgkii* from Teles Pires River (BPP = 0.14). Due to the uncertainty within the *M. schomburgkii* Brazilian and Guiana Shield delimitations with low posterior support, a full range of alternative candidate species is provided in Tab. 6. Among these delimitations, a unified *M. schomburgkii* cluster from the Brazilian and Guiana Shield had the greatest support (BPP = 0.54). Individuals of *M. sauron*, *M. aylan*, and the Brazilian and Guiana Shield *M. schomburgkii* were all monophyletic with posterior clade support value of 1 (Fig. 15). Smallest interspecific genetic distances (Tab. 6) were 0.097 (*M. sauron vs. M. schomburgkii*) and 0.079 (*M. aylan vs. M. schomburgkii*). The distance between *M. sauron* and *M. aylan* was 0.11 (data not shown).

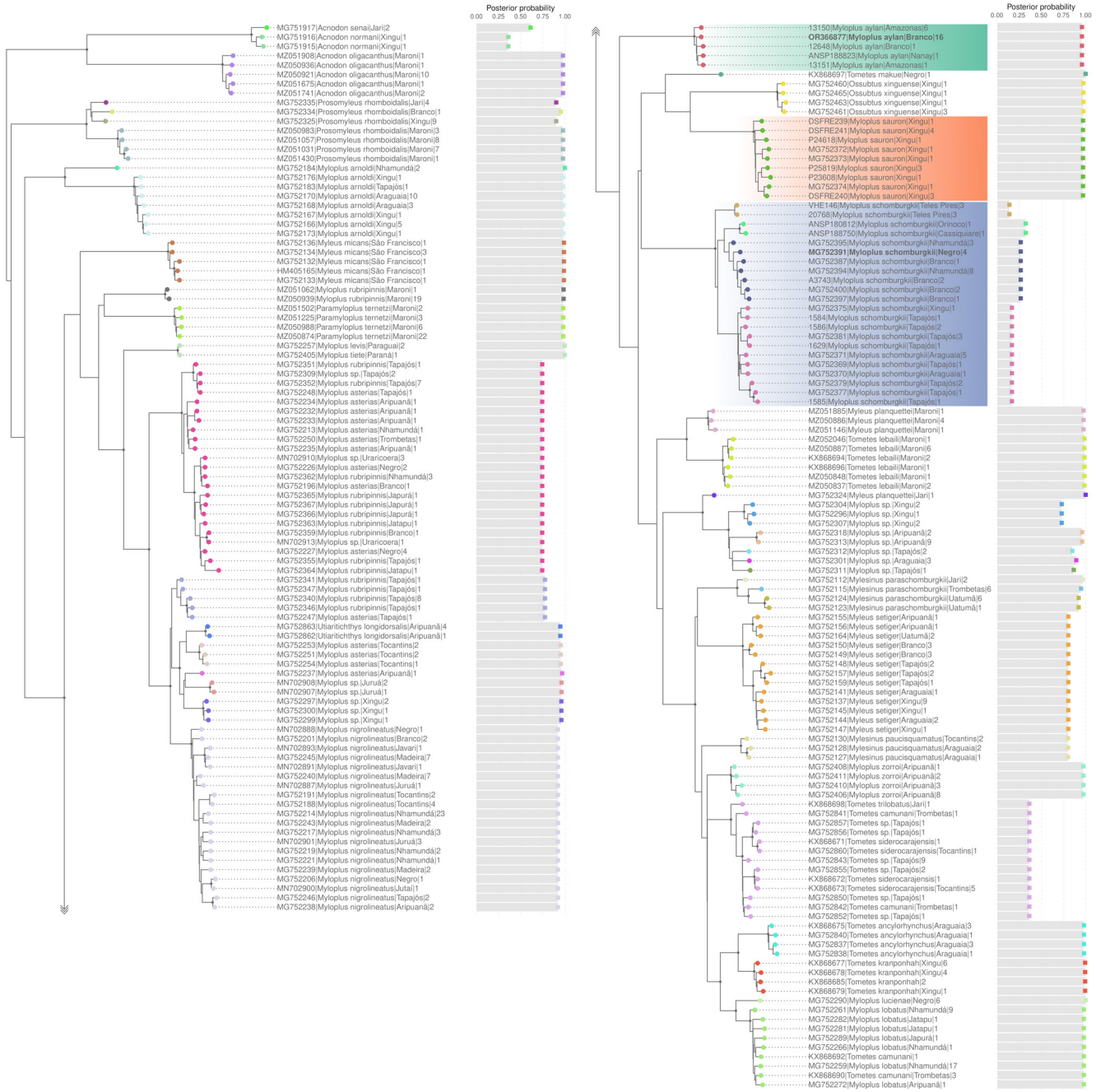

FIGURE 15 | Maximum clade credibility tree obtained from 10,000 post-burnin MrBayes trees. Colored dots represent unique mPTP species delimitation clusters (total 48), with posterior probability for each delimitation reported in the corresponding bar plot (right). Dataset comprised 209 dereplicated COI barcodes. The *Myloplus aylan* samples are highlighted in green, *M. sauron* in orange, and *M. schomburgkii* in blue. Holotype of *M. aylan* and neotype of *M. schomburgkii* highlighted in bold.

TABLE 6 | Summary of alternative species delimitation analyses for geographical candidate species in "*Myloplus schomburgkii*" (*sensu lato*). Posterior probability (speciation) is the frequency of that distinct mPTP delimitation in the posterior subsample of 1,000 MrBayes trees. Posterior probability (monophyly) is the frequency of clade monophyly in the full posterior sample of 10,000 MrBayes trees. Genetic distances (p-distances) were calculated for multiple nested delimitation scenarios, and these are coded 1a-c (three species model), 2a-b (four species model), 3a-d (six species model).

Species	Clade biogeographic subset (delimitation code)	Posterior probability (speciation)	Posterior probability (monophyly)	Max. intraspecific p-distance	Min. interspecific p-distance	Closest interspecific clade
Myloplus sauron	Xingu (1a)	0.97	1	0.01	0.097	1c
Myloplus aylan	Upper Amazon, Madeira, Branco (1b)	0.96	1	0.005	0.079	1c
Myloplus schomburgkii	Brazilian Shield and Guiana Shield (1c)	0.54	1	0.029	0.079	1b
Myloplus schomburgkii	Brazilian Shield including Teles Pires (2a)	0.27	0.66	0.013	0.018	2b
Myloplus schomburgkii	Guiana Shield including Orinoco-Cassiquiare (2b)	0.04	0.47	0.021	0.018	2a
Myloplus schomburgkii	Brazilian Shield excluding Teles Pires (3a)	0.16	0.93	0.009	0.005	3b
Myloplus schomburgkii	Teles Pires (3b)	0.14	0.78	0	0.005	3a
Myloplus schomburgkii	Guiana Shield excluding Orinoco-Cassiquiare (3c)	0.26	0.63	0.008	0.015	3d
Myloplus schomburgkii	Orinoco-Cassiquiare (3d)	0.32	0.99	0.005	0.015	3c

DISCUSSION

Taking an integrative taxonomy approach, this study greatly improves our understanding of species diversity within Serrasalmidae and shows how much it is still underestimated. From the 13 serrasalmids species described in the past decade, more than 30% (four species) were discovered and described using a combination of molecular and morphological data (*e.g.*, Andrade *et al.*, 2017; Escobar *et al.*, 2019; Mateussi *et al.*, 2020; Ota *et al.*, 2020) demonstrating the effectiveness of this methodology to generate robust species hypotheses.

The major challenges in recognition of intraspecific and interspecific limits within Serrasalmidae are the great morphological variation during ontogeny and derived from sexual dimorphism, which has historically caused the description of juveniles, females, and males from the same species as distinct taxa (Zarske, Géry, 1999; Jégu, 2003). This resulted in numerous names and a complex taxonomic history that, together with the lack of taxonomic reviews, complicated our understanding of species-rich genera such as *Serrasalmus* Lacépède 1803, *Metynnis* Cope, 1878, and *Myloplus*.

A geographically widespread investigation using DNA barcoding of over a thousand serrasalmid specimens (Machado *et al.*, 2018) facilitated better understanding of the numerous unrecognized lineages within the family. Two of these lineages, previously identified as *M. schomburgkii*, are described herein. One is *M. sauron* from the Xingu River basin, and the second is *M. aylan* from black and clear water rivers in the central and western Amazon basin comprising the Uatumã, Branco, Nanay, Jutaí, Juruá, Purus and Madeira Rivers. In the Juruá, Purus and Madeira rivers, typical white water rivers, *M. aylan* is found only in black and clear water tributaries of these rivers.

Myloplus schomburgkii has always been easily identified by its unique color pattern, marked by a vertical dark bar in the middle of the flank, popularly known as black-

barred disk pacu, or banda negra in Brazil. This easy recognition hid the diversity within this taxon for a long period. It was even described by Jardine (1841) based on illustrations and comments provided by Robert H. Schomburgk of a female captured in the Rio Negro. Despite several efforts to locate the holotype, it was never found thus, for the species redescription a neotype was designated.

The molecular divergences between the three lineages of the black-barred discus pacu are quite high. *Myloplus schomburgkii* differs from *M. aylan* and *M. sauron* by 7.9% and 9.7%, respectively. Between *M. aylan* and *M. sauron* the distance was even greater, 11%. These percentages of genetic distance are higher than those used by the DNA Barcoding methodology to separate fish species (2% to 3%) and normally represent different taxa (Ward, 2009). This high genetic divergence was the starting point for the investigation of the diversity within this taxon and the consequent description of the two new species of *Myloplus*. This high molecular divergence observed between the three species was corroborated by the morphological characters detailed in the section Diagnosis of each species. The shape of the vertical dark bar can be easily used to distinguish the three species. *Myloplus schomburgkii* has a vertical dark bar with uniform width when compared to the two new species. In *M. sauron* the vertical black bar narrows towards the extremities forming tapered distal tips, while in *M. aylan* the vertical dark bar has a wider region near lateral-line, and extremities do not taper.

We also observed considerable variation in the vertical dark bar in a population of *M. schomburgkii* from the Teles Pires River (upper Tapajós). Individuals from this locality show a short, centralized and rounded black spot, mainly concentrated above the lateral line. This different pattern of the spot led us to consider the presence of a third new species. However, species delimitation support for this group was low (BPP = 0.14) and we could not find any other morphological features to diagnose it from remaining congeners. This low molecular divergence found in the population of Teles Pires, whose pattern of dark bar is the most divergent, may be associated with a recent diversification process, where there has not yet been sufficient accumulation of mutation in the mitochondrial COI gene to molecularly differentiate this taxon using this marker.

Toffoli *et al*. (2008) were also unable to delimit species of stingrays of the genus *Potamotrygon* Garman, 1877 using sequences of the mitochondrial cytochrome c oxidase subunit I gene. The authors attribute the failure to separate the species to the fact that they have not had enough time to reach reciprocal monophyly. *Myloplus schomburgkii* comprised in total four geographically distinct clusters, with a maximum of 2.9% intraspecific genetic divergence, but low species delimitation support for individual groups (BPP < 0.32; Tab. 6). The most evident separation of these clusters appears to be caused by the Solimões-Amazonas system, which has isolated the Guiana and Brazilian shield populations. However, within the Guiana Shield, the cluster of *M. schomburgkii* from the Orinoco-Casiquiare is genetically differentiated from the others, as well as the population from the Teles Pires River in the Brazilian shield, which is also genetically differentiated from other populations of this species. Orinoco-Casiquiare and Teles Pires rivers are the most extreme points north and south, respectively, of this species distribution. However, unlike the Teles Pires population, which has a differentiated and exclusive pattern of the vertical dark bar, the Orinoco-Casiquiare population does not present any morphological feature that distinguishes it from remaining lineages.

Therefore, due to the low species delimitation support and limited morphological evidence at this point, we consider the lineages from Orinoco-Casiquiare and Teles Pires rivers as structured populations from a wide geographic distribution of *M. schomburgkii* from the Guiana and Brazilian shields. Nonetheless, a broader sampling of molecular markers and localities may reveal new insights, and we remain open to the future possibility of recognizing further diversity within this species.

The intraspecific variation within *M. aylan* and *M. sauron* was lower, and no structured populations were recovered in these congeners. *Myloplus aylan* has a more restricted distribution to the western Amazon (*sensu* Dagosta, de Pinna, 2019) and had a maximum intraspecific genetic distance of 0.5% and one species delimitation cluster with high support (BPP = 0.96). *Myloplus sauron*, although even more restricted, occurring only in the Xingu River basin, had an intraspecific genetic distance of 1% and one species delimitation cluster with high support (BPP = 0.97).

Using only one mtDNA marker, our analyses recovered these black-barred disk pacus as paraphyletic but with negligible clade support. Kolmann *et al*. (2020) using an analysis of exon data recovered the well supported monophyly of the three species, with *M. schomburgkii* (Orinoco lineage 1) as sister taxon to *M. aylan* (lineage 3) and *M. sauron* (lineage 2). They corroborated the existence of the three species recognized herein.

The close relationship between the black-barred disk pacus and *Ossubtus* was also found in all recent molecular phylogenies of Serrasalmidae (*i.e*., Kolmann *et al*., 2020; Mateussi *et al*., 2020). This highlighted the complex evolutionary relationships within Myleinae. Despite the elevation of *Paramyloplus* and *Prosomyleus* to generic level by Kolmann *et al*. (2020), the phylogeny of *Myloplus* is far from conclusive. It remains polyphyletic, lacking a proper morphological diagnosis, and several species still await a new generic designation (*e.g*., *M. arnoldi*, *M. lucienae*, and the black-barred pacus). We decided to keep the three species: *M. aylan*, *M. sauron*, and *M. schomburgkii* in *Myloplus* based on the traditional morphological diagnosis of Jégu *et al*. (2004), including the two molariform teeth rows; which present a gap between labial and lingual in premaxilla; and the lack of contact between teeth of premaxillary labial row at the symphysis. We believe, like Mateussi *et al*. (2020), that a more comprehensive study, including all species within the tribe Myleini (or subfamily Myleinae according Kolman *et al*., 2020), can better clarify the generic boundaries, together with their morphological diagnosis, and consequently the intergeneric and interspecific relationships within this group of pacus.

As the three species analyzed here are exploited by ornamental and subsistence commercial fishing, it is necessary that they receive appropriate management accordingly. However, little is known about the dynamics and population status of these pacu species, which makes it difficult to draw up adequate management and conservation plans for each species. It is known that most *Myloplus* species are rheophilic, inhabiting environments with high current, usually in clear or black water rivers (Jégu *et al*., 2004; Andrade *et al*., 2016a,b, 2018b) and have a preference for fruits and seeds for food (Goulding, 1980; Correa *et al*., 2007; Correa, Winemiller, 2014), but little or nothing is known about the genetic structure of populations. Information about the genetic variability of these species and their distribution are important so that the exploitation of the resource does not compromise its continuity.

Comparative material examined. In addition to specimens listed by Andrade *et al*. (2016 a,b, 2018a) and Ota *et al*., 2020. **Brazil:** *Myloplus arnoldi*: INPA 45784, 4, 103.3–112.1 mm SL. *Myloplus asterias*: INPA 26871, 1, 156.0 mm SL; INPA 39331, 1, 171.9 mm SL. *Myleus gurupyensis*: NMW 10589, 175.0 mm SL, syntype. *Myloplus levis*: NUP 13636, 4, 115.8–147.0 mm SL; ZUFMS 4484, 2, 117.8–107.4 mm SL. *Myloplus lobatus*: INPA 53725, 208.2 mm SL. *Myloplus lucienae*: INPA 54771, 1, 167.6 mm SL. *Myloplus planquettei*: INPA 2260, 90.9 mm SL. *Myloplus rhomboidalis*: INPA 40276, 2, 60.8–100.4 mm SL. *Myloplus rubripinnis*: INPA 4549, 2, 156.0–164.2 mm SL; INPA 53087, 2, 141.5–148.2 mm SL. *Myloplus schomburgkii*: INPA 30716, 1, 143.6 mm SL. *Myloplus tiete*: INPA 53243, 1, 43.7 mm SL; ZUFMS 3703, 1, 122 mm SL. *Myloplus torquatus*: INPA 767, 148.1 mm SL; INPA 20013, 2, 68.2–90.1 mm SL; INPA 36702, 1, 77.5 mm SL. *Myloplus zorroi*: INPA 50880, holotype, 1, 326.2 mm SL. *Tometes maculatus*: MZUSP 3356, holotype, 168.3 mm SL. **French Guiana:** *Myloplus ternetzi*: INPA 3037, 2, 77.7–84.0 mm SL.

ACKNOWLEDGMENTS

We would like to thank Romério Briglia Ferreira (ICMBio-RR) and José Gregório Martínez (COLMAYOR) for the logistical support during the collections in the Branco and Orinoco rivers respectively; Mario Nunes (UFAM) for help in editing the map; Aline Ximenes (UFAM) for assistance with laboratory procedures; Marcelo Rocha (UEA) for the effort in catching a mature specimen for the holotype of *Myloplus aylan*; Lucia Rapp Py-Daniel (INPA) for the museum support and providing the pictures of *M. aylan*; Mark Sabaj (ANSP) for providing the pictures of color in life of *M. sauron*; Isaac Sidomar (UFPA) for the help with image editing; Gabriel Deprá (NUP) for the help with image editing and for the suggestion on parts of the manuscript and Kevin Morgan-Ruiz, IIAP curator. We also would like to express our gratitude to the reviewers Lucia Rapp Py-Daniel, José Birindelli (UEL) and Juan M. Mirande (CONICET), as well as to the editor Bruno Melo (AMNH), for their comments and contributions to this manuscript. VDP is grateful to the Coordenação de Aperfeiçoamento de Pessoal de Nível Superior (CAPES) for receiving a scholarship (Grant #88887.678154/2022c00). MÂ is funded by the Conselho Nacional de Desenvolvimento Científico e Tecnológico (CNPq #310522/2023–4).

REFERENCES

- **Andrade MC, Jégu M, Buckup PA, Netto-Ferreira AL.** A new *Myleus* species (Characiformes: Serrasalmidae) from the rio Tapajós basin, Brazil. J Fish Biol. 2018a; 92(6):1902–14. https://doi.org/10.1111/jfb.13628
- **Andrade MC, Jégu M, Giarrizzo T.** *Tometes kranponhah* and *Tometes ancylorhynchus* (Characiformes: Serrasalmidae), two new phytophagous serrasalmids, and the first *Tometes* species described from the Brazilian Shield. J Fish Biol. 2016a; 89(1):467–94. https://doi:10.1111/jfb.12868
- **Andrade MC, Jégu M, Giarrizzo T.** A new large species of *Myloplus* (Characiformes, Serrasalmidae) from the rio Madeira basin, Brazil. Zookeys. 2016b; 571:153–67. https://doi.org/10.3897/zookeys.571.5983
- **Andrade MC, López-Fernández H, Liverpool EA.** New *Myloplus* from Essequibo River basin, Guyana, with discussion on the taxonomic status of *Myleus pacu* (Characiformes: Serrasalmidae). Neotrop Ichthyol. 2019; 17(4):e190026. https://doi.org.10.1590/1982-0224-20190026

- **Andrade MC, Machado VN, Jégu M, Farias IP, Giarrizzo T.** A new species of *Tometes* Valenciennes 1850 (Characiformes: Serrasalmidae) from Tocantins-Araguaia River Basin based on integrative analysis of molecular and morphological data. PLoS ONE. 2017; 12(4):e0170053. https://doi.org/10.1371/journal.pone.0170053
- **Andrade MC, Ota RP, Bastos DA, Jégu M.** A new large *Myloplus* Gill 1896 from rio Negro basin, Brazilian Amazon (Characiformes: Serrasalmidae). Zootaxa. 2018b; 4205(6):571–80. https://doi.org/10.11646/zootaxa.4205.6.5
- **Boeseman M.** Notes on South American catfishes, including remarks on Valenciennes and Bleeker types in the Leiden Museum. Zool Meded. 1972; 47(23):293–320.
- **Brown SDJ, Collins RA, Boyer S, Lefort M-C, Malumbres-Olarte J, Vink CJ *et al*.** Spider: an R package for the analysis of species identity and evolution, with particular reference to DNA barcoding. Mol Ecol Resour. 2012; 12(3):562–65. https://doi.org/10.1111/j.1755-0998.2011.03108.x
- **Castello L, Macedo MN.** Large-scale degradation of Amazonian freshwater ecosystems. Glob Chang Biol. 2016; 22(3):990–1007. https://doi.org/10.1111/gcb.13173
- **Correa SB, Winemiller KO, López-Fernández H, Galetti M.** Evolutionary perspectives on seed consumption and dispersal by fishes. Bioscience. 2007; 57(9):748–56. https://doi.org/10.1641/B570907
- **Correa SB, Winemiller KO.** Niche partitioning among frugivorous fishes in response to fluctuating resources in the Amazonian floodplain forest. Ecology. 2014; 95(1):210–24. https://doi.org/10.1890/13-0393.1
- **Dagosta FCP, de Pinna M.** The fishes of the Amazon: distribution and biogeographical patterns, with a comprehensive list of species. Bull Am Mus Nat. 2019; 413(2019):1–163. https://doi.org/10.1206/0003-0090.431.1.1
- **Darriba D, Taboada GL, Doallo R, Posada D.** jModelTest 2: more models, new heuristics and parallel computing. Nat Methods. 2012; 9:772. https://doi.org/10.1038/nmeth.2109
- **Dary EP, Ferreira E, Zuanon J, Röpke CP.** Diet and trophic structure of the fish assemblage in the midcourse of the Teles Pires River, Tapajós River basin, Brazil. Neotrop Ichthyol. 2017; 15(4):e160173. https://doi.org/10.1590/1982-0224-20160173
- **Eigenmann CH.** Catalogue of the freshwater fishes of tropical and south temperate America. Reports of the Princeton University Expeditions to Patagonia 1896–1899. Zoology. Fishes Patagonia. 1910; 3(4):375–511. https://doi.org/10.5962/bhl.title.2097
- **Eigenmann CH.** The freshwater fishes of British Guiana, including a study of the ecological grouping of species and the relation of the fauna of the plateau to that of the lowlands. Mem Carnegie Mus. 1912; 5(1):1–578.
- **Eigenmann CH.** The Serrasalminae and Mylinae. Ann Carnegie Mus. 1915; 9(3–4):225–72.
- **Escobar L. MD, Ota RP, Machado-Allison A, Andrade-López J, Farias IP, Hrbek T.** A new species of *Piaractus* (Characiformes: Serrasalmidae) from the Orinoco Basin with a redescription *of Piaractus brachypomus*. J Fish Biol. 2019; 95(2):411–27. https://doi.org/10.1111/jfb.13990
- **Fitzgerald DB, Sabaj-Pérez MH, Sousa LM, Gonçalves AP, Rapp Py-Daniel LH, Lujan NK *et al*.** Diversity and community structure of rapids-dwelling fishes of the Xingu River: Implications for conservation amid large-scale hydroelectric development. Biol Conserv. 2018; 222:104–12. https://doi: 10.1016/j.biocon.2018.04.002
- **Fitzgerald DB, Winemiller KO, Sabaj-Pérez MH, Sousa LM.** Seasonal changes in the assembly mechanisms structuring tropical fish communities. Ecology. 2017; 98(1):21–31. https://doi.org/10.1002/ecy.1616
- **Fricke R, Eschmeyer WN, Van der Laan R.** Eschmeyer's catalog of fishes: genera, species, references [Internet]. San Francisco: California Academy of Science; 2023. Available from: http://researcharchive.calacademy.org/research/ichthyology/catalog/fishcatmain.asp
- **García-Dávila C, Ruiz-Tafur M, Sánchez H, Flores M, Mejia J, Angulo C *et al*.** Guía de identificación de peces de consumo de la Amazonía peruana. Iquitos: Instituto de Investigaciones de la Amazonía Peruana; 2022.

- **Géry J.** Characoids of the World. Neptune City, New Jersey: T.F.H. Publications; 1977.
- **Géry J.** The Serrasalmidae (Pisces, Characoidei) from the Serra do Roncador, Mato Grosso, Brasil. Amazoniana. 1979; 6(4):467–95.
- **Gosline WA.** Notes on the Characid fishes of the subfamily Serrasalminae. Proc Calif Acad Sci. 1951; 27(2):17–64.
- **Goulding M.** The fishes and the forest: explorations in Amazonian natural history. Berkeley: University of California Press; 1980.
- **International Union for Conservation of Nature (IUCN). Standards and Petitions Subcommittee.** Guidelines for using the IUCN Red List categories and criteria. Version 15.1 [Internet]. Gland; 2022. Available from: http://www.iucnredlist.org/resources/redlistguidelines
- **Isaac VJ, Almeida MC, Cruz REA, Nunes LG.** Artisanal fisheries of the Xingu River basin in Brazilian Amazon. Braz J Biol. 2015; 75(3):125–37. http://dx.doi.org/10.1590/1519-6984.00314BM
- **Jardine W, Schomburgk RH.** The natural history of fishes of Guiana. Part. 1. Edinburgh: W. H. lizars; 1841. https://doi.org/10.5962/bhl.title.15849
- **Jégu M.** *Ossubtus xinguense*, nouveaux genre et espéce du Rio Xingu, Amazonie, Brésil (Teleostei: Serrasalminae). Ichthyol Explor Freshw. 1992; 3:235–52.
- **Jégu M.** Subfamily Serrasalminae (Pacus and Piranhas). In: Reis RE, Kullander SO, Ferraris CJ, Jr., editors. Check list of the freshwater fishes of South and Central America. Porto Alegre: Edipucrs; 2003. p.182–96.
- **Jégu M, Hubert N, Belmont-Jegu E.** Réhabilitation de *Myloplus asterias* (Müller & Troschel, 1844), espèce-type de *Myloplus* Gill, 1896 et validation du genre *Myloplus* Gill (Characidae: Serrasalminae). Cybium. 2004; 28(2):119–57. https://doi.org/10.26028/cybium/2004-282-005
- **Jégu M, Keith P, Le Bail P-Y.** *Myloplus planquettei* sp. n. (Teleostei, Characidae), une nouvelle espèce de grand Serrasalminae phytophage du bouclier guyanais. Rev Suisse Zool. 2003; 110(4):833–53. https://doi.org/10.5962/bhl.part.80216
- **Jégu M, Santos GM.** Révision du statut de *Myleus setiger* Müller et Troschel, 1844 et de *Myleus knerii* (Steindachner, 1881) (Teleostei: Characidae: Serrasalminae) avec une description complémentaire des deux espèces. Cybium. 2002; 26(1):33–57.
- **Kapli P, Lutteropp S, Zhang J, Kobert K, Pavlidis P, Stamatakis A *et al*.** Multi-rate Poisson tree processes for single-locus species delimitation under maximum likelihood and Markov chain Monte Carlo. Bioinformatics. 2017; 33(11):1630–38. https://doi.org/10.1093/bioinformatics/btx025
- **Katoh K, Standley DM.** MAFFT multiple sequence alignment software version 7: improvements in performance and usability. Mol Biol Evol. 2013; 30(4):772–80. https://doi.org/10.1093/molbev/mst010
- **Kearse M, Moir R, Wilson A, Stones-Havas S, Cheung M, Sturrock S *et al*.** Geneious Basic: an integrated and extendable desktop software platform for the organization and analysis of sequence data. Bioinformatics. 2012; 28(2):1647–49. https://doi.org/10.1093/bioinformatics/bts199
- **Kner R.** Zur Familie der Characinen. III. Fölge. Der Ichthyologischen Beiträge. Denkschr K Akad Wiss Wien. 1860; 17:9–62.
- **Kolmann MA, Hughes LC, Hernandez LP, Arcila D, Betancur-R R, Sabaj MH *et al*.** Phylogenomics of piranhas and pacus (Serrasalmidae) uncovers how dietary convergence and parallelism obfuscate traditional morphological taxonomy. Syst Biol. 2020; 70(3):576–92. https://doi.org/10.1093/sysbio/syaa065
- **Machado VN, Collins RA, Ota RP, Andrade MC, Farias IP, Hrbek T.** One thousand DNA barcodes of piranhas and pacus reveal geographic structure and unrecognized diversity in the Amazon. Sci Rep. 2018; 8:8387. https://doi.org/10.1038/s41598-018-26550-x
- **Machado-Allison A, Fink W.** Sinopsis de las especies de la subfamilia Serrasalminae presentes en la cuenca del Orinoco. Claves, diagnosis e ilustraciones. Caracas: Universidad Central de Venezuela; 1995.

- **Mateussi NTB, Melo BF, Ota RP, Roxo FF, Ochoa LE, Foresti F *et al*.** Phylogenomics of the Neotropical fish family Serrasalmidae with a novel intrafamilial classification (Teleostei: Characiformes). Mol Phylogenet Evol. 2020; 153:106945. https://doi.org/10.1016/j.ympev.2020.106945
- **Mattox GMT, Britz R, Toledo-Piza M.** Skeletal development and ossification sequence of the characiform *Salminus brasiliensis* (Ostariophysi: Characidae). Ichthyol Explor Freshw. 2014; 25(2):103–58.
- **Müller J, Troschel FH.** Synopsis generum et specierum familiae Characinorum (Prodo mus description is novorum generum et specierum). Arch Naturgesch. 1844; 10(1):81–99.
- **Müller J, Troschel FH.** Horae ichthyologicae. Beschreibung und Abbildungneuer Fische. Die Familie der Characinen. Erstes Zweites Heft. Berlin: Veit & Comp; 1845; 1–40. https://doi.org/10.5962/bhl.title.6935
- **Murrieta-Morey GA, Aliano AMB, Grandez FAG.** New species of Dactylogyridae Bychowsky, 1933 infecting the gills of *Myloplus schomburgkii* (Jardine) and *Colossoma macropomum* (Cuvier) in the Peruvian Amazon. Syst Parasitol. 2019 96:511–19. https://doi.org/10.1007/s11230-019-09865-9
- **Murrieta-Morey GA, Satalaya-Arellano H, Ramírez-Chirinoz CS, Rodríguez-Chu SA.** Mortality of black-band *Myloplus schomburgkii* due to poor water quality associated with overpopulation of duckweeds in a culture pond in the peruvian Amazonia. Folia Amaz. 2021; 30(1):107–12. https://doi.org/10.24841/fa.v30i1.543
- **Norman JR.** The South American characid fishes of the subfamily Serrasalmoninae, with a revision of the genus *Serrasalmus* Lacepède. Proc Zool Soc London. 1929; 98(52):781–829.
- **Nyholt K, Jardine TD, Villamarín F, Jacobi CM, Hawes JE, Campos-Silva JV *et al*.** High rates of mercury biomagnification in fish from Amazonian floodplain-lake food webs. Sci Total Environ. 2022; 883:155161. https://doi.org/10.1016/j.scitotenv.2022.155161
- **Ohara WM, Lima FCT, Salvador GN, Andrade MC.** Peixes do rio Teles Pires: Diversidade e guia de identificação. Aparecida de Goiânia: Gráfica Amazonas e Editora Ltda; 2017.
- **Ortí G, Petry P, Porto JIR, Jegu M, Meyer A.** Patterns of nucleotide change in mitochondrial ribosomal RNA genes and the phylogeny of piranhas. J Mol Evol. 1996; 42:169–82.
- **Ortí G, Sivasundar A, Dietz K, Jégu M.** Phylogeny of the Serrasalmidae (Characiformes) based on mitochondrial DNA sequences. Genet Mol Biol. 2008; 31(1):343–51. https://www.scielo.br/j/gmb/a/WQBqC-6FyNFCmFPqwN8jmXXh/?format=pdf&lang=en
- **Ota RP, Machado VN, Andrade MC, Collins RA, Farias IP, Hrbek T.** Integrative taxonomy reveals a new species of pacu (Characiformes: Serrasalmidae: *Myloplus*) from the Brazilian Amazon. Neotrop Ichthyol. 2020; 18(1):e190112. https://doi.org/10.1590/1982-0224-20190112
- **Papa Y, Le Bail P-Y, Covain R.** Genetic landscape clustering of a large DNA barcoding data set reveals shared patterns of genetic divergence among freshwater fishes of the Maroni basin. Mol Ecol Resour. 2021; 21(6):2109–24. https://doi.org/10.1111/1755-0998.13402
- **Paradis E, Schliep K.** APE 5.0: an environment for modern phylogenetics and evolutionary analyses in R. Bioinformatics. 2019; 35(3):526–28. https://doi.org/10.1093/bioinformatics/btg412
- **Peru.** Decreto Supremo Nº 15, de 30 de abril de 2009. Decreto Supremo que Aprueba el Reglamento de Ordenamiento Pesquero de la Amazonía Peruana. Ministerio de la Produccion, Lima, Peru; 2009.
- **Prang G.** An industry analysis of the freshwater ornamental fishery with particular reference to the supply of Brazilian freshwater ornamentals to the UK market. Scient Mag Uakari. 2007; 3(1):7–51.
- **Ragazzo MTP.** Peixes do rio Negro = Fishes of rio Negro: Alfred Russel Wallace. São Paulo: EDUSP; 2002.
- **Ríos-Villamizar EA, Piedade MTF, Costa JG, Adeney JM, Junk WJ.** Chemistry of different Amazonian water types for river classification: a preliminary review WIT. WIT Trans Ecol Environ. 2014; 178:17–28. https://doi.org/10.2495/13WS0021

- **Ríos-Villamizar EA, Adeney JM, Junk WJ, Piedade MTF.** Physicochemical features of Amazonian water typologies for water resources management. IOP Conf Ser Earth Environ Sci. 2020; 427:012003. https://doi.org/10.1088/1755-1315/427/1/012003
- **Ronquist F, Teslenko M, Van der Mark P, Ayres DL, Darling A, Höhna S *et al*.** MrBayes 3.2: efficient Bayesian phylogenetic inference and model choice across a large model space. Syst Biol. 2012; 61(3):539–42. https://doi.org/10.1093/sysbio/sys029
- **Schliep KP.** Phangorn: phylogenetic analysis in R. Bioinformatics. 2011; 27(4):592–93. https://doi.org/10.1093/bioinformatics/btq706
- **Silvano RAM, Nitschke PP, Vieira KC, Nagl P, Martínez ATR, Chuctaya JA et al.** Atlas of fishes od Tapajós and Negro rivers I: Characiformes. In: Silvano RA, editor. Fish and fisheries in the Brazilian Amazon. Springer, Cham; 2020. p.41–196. https://doi.org/10.1007/978-3-030-49146-8_4
- **Sioli H.** The Amazon: limnology and landscape ecology of a mighty tropical river and its basin. Dordrecht: Dr. W. Junk Publishers; Monographiae Biologicae, 56; 1984.
- **Steindachner F.** Ichthyologische Beiträge (V). SitzBer K Akad Wiss Math Naturwiss Kl. 1876; 74:49–240.
- **Thompson AW, Betancur-RR, López-Fernández H, Ortí G.** A time-calibrated, multi-locus phylogeny of piranhas and pacus (Characiformes: Serrasalmidae) and a comparison of species tree methods. Mol Phylogenet Evol. 2014; 81:242–57. http://dx.doi.org/10.1016/j.ympev.2014.06.018
- **Valenciennes A.** Tome vingt-deuxième. Suitedu livre vingt-deuxième. Suite de la familledes Salmonoïdes. Table générale de l'Histoire Naturelle des Poissons. Histoire naturelle des poissons. 1850; 22:1–91.
- **Vasconcellos ACS, Ferreira SRB, Sousa CC, Oliveira MW, Oliveira ML, Basta PC.** Health Risk Assessment Attributed to Consumption of Fish Contaminated with Mercury in the Rio Branco Basin, Roraima, Amazon, Brazil. Toxics. 2022; 10(9):516. https://doi.org/10.3390/toxics10090516
- **Venticinque E, Forsberg B, Barthem R, Petry P, Hess L, Mercado A *et al*.** An explicit GIS-based river basin framework for aquatic ecosystem conservation in the Amazon. Earth Syst Sci. 2016; 8(2):651–61. https://doi.org/10.5194/essd-8-651-2016
- **Ward RD.** DNA barcode divergence among species and genera of birds and fishes. Mol Ecol Resour. 2009; 9(4):1077–85. https://doi.org/10.1111/j.1755-0998.2009.02541.x
- **Winemiller KO, McIntyre PB, Castello L, Fluet-Chouinard E, Giarrizzo T, Nam S *et al*.** Balancing hydropower and biodiversity in the Amazon, Congo, and Mekong. Science. 2016; 351(6269):128–29. https://10.1126/science.aac7082
- **Zarske A, Géry J.** Revision der neotropischengattung *Metynnis* Cope, 1878. 1. Evalution der typusexemplare der nominellenarten (Teleostei: Characiformes: Serrasalmidae). Zool Abh Staatl Mus Tierk Dresden. 1999; 50:169–216.
- **Zarske A.** Das Typusmaterial der Characiformes des Museums für Naturkundezu Berlin. Teil 2b (3). Südamerikanische Characiformes imweiteren Sinne (Teleostei: Ostariophysi: Characiformes: Serrasalmidae, Acestrorhynchidae, Erythrinidae, Lebiasinidae). Vertebr Zool. 2012; 62(1):19–77.
- **Zhang C, Rannala B, Yang Z.** Robustness of compound Dirichlet priors for Bayesian inference of branch lengths. Syst Biol. 2012; 61(5):779–84. https://doi.org/10.1093/sysbio/sys030

AUTHORS' CONTRIBUTION

Valéria N. Machado: Conceptualization, Data curation, Formal analysis, Investigation, Methodology, Project administration, Writing-original draft, Writing-review and editing.
Victória D. Pereira: Conceptualization, Data curation, Formal analysis, Investigation, Methodology, Project administration, Writing-original draft, Writing-review and editing.
Rafaela P. Ota: Conceptualization, Data curation, Formal analysis, Investigation, Methodology, Project administration, Writing-original draft, Writing-review and editing.
Rupert A. Collins: Data curation, Formal analysis, Investigation, Methodology, Writing-original draft, Writing-review and editing.
Marcelo Ândrade: Data curation, Investigation, Methodology, Writing-review and editing.
James R. Garcia-Ayala: Data curation, Formal analysis, Investigation, Methodology, Writing-review and editing.
Michel Jégu: Formal analysis, Investigation, Methodology, Writing-review and editing.
Izeni P. Farias: Funding acquisition, Investigation, Methodology, Resources, Writing-review and editing.
Tomas Hrbek: Funding acquisition, Investigation, Methodology, Resources, Writing-review and editing.

ETHICAL STATEMENT

Permanent IBAMA License number 11325–1.

COMPETING INTERESTS

The author declares no competing interests.

HOW TO CITE THIS ARTICLE

- **Machado VN, Pereira VD, Ota RP, Collins RA, Ândrade M, Garcia-Ayala JR, Jégu M, Farias IP, Hrbek T.** Integrative taxonomy of the black-barred disk pacus (Characiformes: Serrasalmidae), including the redescription of *Myloplus schomburgkii* and the description of two new species. Neotrop Ichthyol. 2024; 22(1):e230095. https://doi.org/10.1590/1982-0224-2023-0095

Neotropical Ichthyology

OPEN ACCESS

SBI
Official Journal of the
Sociedade Brasileira de Ictiologia